NEW CONCEPTS IN OCTANE BOOSTING OF FUELS FOR INTERNAL COMBUSTION ENGINES

Paul F. Waters
Department of Chemistry, American University
4400 Mass. Ave. NW, Washington, DC 20016
and
Jerry C. Trippe
General Technology Applications, Inc.
7400 Gallerher Road, Gainesville, VA 21055

KEYWORDS: polymer, droplet size, octane increase

ABSTRACT
The holy grail of the combustion of fuels in internal combustion engines is the perfect mixture of fuel and air. This ideal state will allow complete combustion at a uniform rate, delivering optimal power with no harmful emissions under all operating conditions. A primary objective of engine builders is to achieve engine designs that will produce a uniform distribution of very-small-diameter fuel droplets, said to be crucial to forming a mixture approaching perfection. When high molecular weight polymers are added to hydrocarbon fuels at low ppm levels, the viscoelasticity manifested during the stress of carburetion or injection precludes the formation of large numbers of fine droplets. The average droplet size of such fuels, aerosolized in air, is measurably larger than the droplets sprayed with neat fuels, and the size distribution is narrowed. Moreover, the number of droplets below the upper threshold for explosive combustion is greatly reduced. Such polymer-fortified fuels burn at substantially lower average temperatures, thereby increasing the octane rating of the fuel, the efficiency of combustion, and the power delivered to the crankshaft.

INTRODUCTION

The combustion of hydrocarbon (HC) fuel in internal combustion (IC) engines is an extremely complex event, encompassing many variables, and far from being completely understood. It is a phenomenon which is readily characterized by the adage, "The less known about a scientific or engineering process, the more measurements required to define it." In support of this view, a partial listing of topics on the combustion of gasoline in IC engines, which appeared in publications of the Society of Automotive Engineers over the last decade, includes: the properties of spray from an injector, the location and focusing of injectors, the time of injection relative to intake valve position, the flow of the air/fuel mixture in the induction channel, the liquid fuel films on the walls of the induction channel and the intake valve, the vaporization of droplets in the induction channel, the vaporization of the wall film in the induction channel, the atomization of the wall film from the induction channel caused by air flow, the fuel species which comprise the wall film of the induction channel, the effects of viscosity and surface tension on the air-stripping of fuel from the wall film of the induction channel, the fuel from one injection remaining in the induction channel through multiple cycles, the condition of the air/fuel mixture in the cylinders, the liquid fuel film on the walls of the cylinders, the spatial distribution of the fuel species in the gas in the cylinders, the effects of swirl and tumble motions in the cylinders, the presence of liquid fuel at the end of compression, the stratification of the fuel/air charge, the air/fuel ratio at the spark plug, the condition of the air/fuel mixture at ignition, the carryover of unburned fuel in the cylinders from the previous exhaust stroke, and the charge temperature. Many of these factors have been investigated over a range of operating conditions and then related to ignition, inflammation, rate of heat release, burning time, mean effective pressure, cycle variability, end-gas temperature, knock, emissions and volumetric efficiency.

The segment of the combustion process addressed in this paper is the air/fuel mixture preparation, a critical component of the overall process, which affects virtually all of the variables listed above. The air/fuel mixture preparation involves the introduction of the gasoline into the induction system from a carburetor or an injector, the mixing of the air and fuel in the induction channel, the transport of the air/fuel mixture into the cylinder during the intake stroke, the compression of the mixture, and the condition of the mixture at the time of ignition.

It is the physical properties of the gasoline which constitute the greatest single barrier to providing an optimal air/fuel charge at the spark plug at the time of ignition. A description is given here, and a model is proposed, for the manner in which polymers alter the physical properties of gasoline droplets. Polymers improve the combustion process, and lead to increases in fuel octane rating, power production and volumetric efficiency, as well as substantial emissions reductions. Analogous benefits have been found with low ppm concentrations of polymers in diesel fuel, burned in both large and small diesel engines, where the release of black particulates is greatly diminished. The most dramatic improvements have been recorded with the polymer-fortified fuels used in two-cycle engines, where the usual raw-gas emissions are significantly curtailed and noise is abated.

EXPERIMENTAL

VISCOELASTICITY

When elastomers of molecular weight, sufficient to impart a viscoelasticity at low concentrations, are added to gasoline, a hydrodynamic control is conferred upon the fuel. A quiescent viscoelastic fluid acts as an ordinary liquid. Under sudden stress, the liquid exhibits greatly increased viscosity and solid-like elastic properties. The effect of viscoelasticity on the aerosolization of fuels is shown in Figure 1, where an antimisting function, $P/(P - R)$ is plotted against both the molecular weight and the concentration of polyisobutylene in diesel fuel at 20° C (●). P is the quantity per minute of liquid pumped through a paint sprayer; R is the quantity of liquid recovered in a line-of-sight vessel, positioned two meters from the sprayer (1). In a correlative experiment, the function, h/c, is plotted against the molecular weight of polyisobutylene in toluene at 20° C (O). The term, h, is the height to which a thin stream of viscoelastic solution may be stretched before separation occurs, and c is the concentration (2). Polyisobutylene, of molecular weight 7.2 Md, was used in all of the measurements reported here.

TEMPERATURE

Table 1 contains measurements recorded at the D.A.M. engine lab in Duchess County, NY, on a four-cycle, single-cylinder Briggs & Stratton gasoline engine. The fuel contained 10 ppm of polymer. The data are representative of the temperature decreases observed in both gasoline and diesel engines using polymer-fortified fuels. A relation developed between the temperature of the unburned gas in a gasoline engine and the octane requirement, measured on a 2.2 liter, 4-cylinder, Chrysler production engine, is that for each 7° K increase in unburned gas temperature, the octane requirement of the fuel increases by a single unit (3). If a substance decreases the operating temperature of an engine, this is tantamount to increasing the octane rating of the fuel-in-use. Such a substance would not necessarily exhibit an octane increase when tested at constant temperature.

POWER

In Figure 2 are presented test data recorded on a 1990 turbodiesel Toyota Landcruiser with a 400,000 km odometer reading, in Perth, Australia. The dynamometer measurement of horsepower (BHP) was first determined without polymer in the fuel. The peak BHP was 95.7. Polymer was added to achieve a concentration of 10 ppm, and the vehicle was returned four days later for testing. The 107.2 BHP recorded represents a 12 % increase in power attributable to the polymer [in order to save space the neat fuel value was traced into Figure 2 from the DYNO DYNAMICS dynamometer graph].

EMISSIONS

As a consequence of the overall decrease in operating temperatures, and the control of the droplet size and size distribution, the emissions of the routinely-monitored pollutants from gasoline engines are reduced substantially by the addition of 10 ppm of polymer to the gasoline. The first three entries in Table 2 were measured by engineers from SNAP-ON TOOL INC., in Richmond, VA; the last two were determined at an official State of Virginia testing facility in Fairfax County, VA.

TRANSIENTS

The values given in Figure 3 were measured by engineers from EG&G AUTOMOTIVE RESEARCH, INC., in San Antonio, TX, on a 1985 Nissan 300 ZX, with a gasoline engine and an odometer reading of 180,000 miles. The dark bars show the mass of neat fuel required to attain a given MPH; the light bars, the mass of fuel containing the polymer at 10 ppm required to reach comparable speeds. The polymer has a profound effect on the efficiency of combustion during accelerations, where engines are least efficient, and the emissions of pollutant species are greatest—the conditions frequently met in urban driving.

PARTICLE SIZE AND DENSITY

Figure 4 shows photographs of aerosols, produced by a paint sprayer, taken at the University of Dayton, Dayton, OH. The probing technique used was laser light scattering. In order to avoid a possible explosion from the mist, which would be produced with raw gasoline, water and an aqueous solution of high molecular weight polyethylene oxide were sprayed. The solution was identical in viscoelastic properties to a solution of polyisobutylene in gasoline at 10 ppm, measured with the ductless siphon (2). The dark region depicts water, with its high density of minute droplets; the light region shows the droplets from the polymer solution. The marker is a 50-micron copper wire.

DISCUSSION

Gasoline contains species which vaporize at different rates, at a given temperature. In neat fuel, the "light" ends vaporize more rapidly, and concentrate near the spark plug at ignition. The "heavy" ends dominate the liquid films in the induction channel, and on the cylinder walls, and remain further from the spark plug at ignition. The "light" paraffin molecules burn more rapidly than the "heavy" aromatic molecules. The ignition of the "light" molecules causes an early temperature spike which dissociates Nitrogen molecules and generates NO_x. The predominance of the "heavy" ends in the unburned fuel causes a relatively slow flame-front advance, and these ends may persist beyond exhaust valve opening. This model leads to: knock, poor effective pressure, unburned HC, CO, partially oxidized HC, NO_x and particulates.

The viscoelastic effect displayed in Figure 1 demonstrates that, at sufficiently high molecular weight, the polymer is a strong deterrent to mist formation. Very little fuel is lost at the higher concentrations sprayed. In usable fuels, the concentration is two orders of magnitude lower, so the polymer can permit appropriate droplet formation. The polymer is able to achieve the beneficial results reported here by limiting the population of very-small-diameter droplets (Figure 4). In addition, the droplets formed possess a certain toughness. The larger size, and inelastic structure, provide the momentum for further penetration of the fuel droplets into the faster moving air mass, thereby producing an air/fuel mixture closer to the ideal. Moreover, under stress, the polymer conveys to the droplets a surface viscoelasticity which increases the surface tension, and limits the vaporization of the "light" ends from the droplets throughout the stress, and until such time as the polymer molecules relax. The composition of the fuel droplets should remain relatively uniform during the relaxation. As the droplets are heated, at the point of relaxation, the vaporization of all species, through the surface film, is likely to be spontaneous, leading to a more uniform distribution of the various gaseous species in the air/fuel mixture.

The polymer-containing fuels reduce the temperature, as reported in Table 1, and result in antiknock activity and an octane increase. This suggests that a more homogeneous blend exists at ignition, and that the high temperature spike, which causes knock, is moderated, and this implies an improved air/fuel mixture preparation. Moreover, exhaust temperatures are lower with polymer-fortified fuels. High exhaust temperatures are produced by fuels burning late into the expansion stroke. A more uniform blend of "light" and "heavy" species in the unburned gas, ahead of the flame front, results in faster flame advance, and lower exhaust temperatures. The exhaust temperature differentials, entered in Table 1, indicate better air/fuel mixture preparation. Likewise, the power increase, displayed in Figure 2, can develop only with an increase in the octane (cetane here) rating of the fuel, suggesting a more homogeneous air/fuel mixture preparation. The reduction of the pollutants HC and CO, reported in Table 2, reflects a more complete combustion, and the decrease in NO_x relates to the paucity of fine fuel droplets. These environmental improvements, together, imply an air/fuel mixture preparation nearer to the ideal.

As revealed in Figure 3, the fortified fuel is particularly effective in overcoming inefficiencies during transients. The cause of transient hesitations is the build-up of the liquid-fuel film in the induction channel. The consensus is that it is the inability of this film to vaporize rapidly enough to be readily transported into the cylinder, when the intake valve opens, that is the cause of the lean mixture and the hesitation. It is counterintuitive to believe that a substance which limits vaporization from the droplets in the cylinders, as suggested here, could improve engine performance during transients, when limited vaporization from the liquid-fuel film in the induction channel is the cause of the hesitation. The results from the EG&G tests, however, are quite convincing. A reconsideration of the problem is instructive. The paradigm proposed here is: 1) the transient hesitations arise because, with neat fuels, there is insufficient fuel, either in the liquid or vapor phase, imported into the cylinder; 2) the inelastic droplets of fortified fuels, which exist before the polymer reaches complete relaxation, rebound from the induction channel walls in sufficient numbers to reduce the portion of liquid film on the walls, and increase the concentration of liquid droplets in the air/fuel mixture; 3) the polymer limits vaporization from the fuel droplets in the air/fuel mixture flowing in the induction channel, and these fuel-dense droplets are available for transport into the cylinder when the intake valve opens. This model is satisfactory for understanding the improvement of engine performance during transients and in steady-state combustion as well.

CONCLUSIONS

High molecular weight polymers confer significant benefits when present in fuels burned in IC engines. The overall operating temperatures are decreased, imputing an octane or cetane rating increase to the fuel-in-use. The power output is increased. Fuel consumption is reduced and, while not reported explicitly here, mileage gains are substantial, particularly with diesel and two-cycle, engine-powered vehicles (4). The pollutants, HC, CO and NO_x are reduced.

ACKNOWLEDGEMENT

We thank John B. Waters for providing the computer graphics.

REFERENCES

(1) Waters, P.F., Hadermann, A.F. and Trippe, J.C., Proceedings of the Second International Conference on Reactive Processing of Polymers, pp 11-22, J.T. Lindt, Ed., U. of Pittsburgh, Pittsburgh, PA, November 2-4, 1982.

(2) Chao, K.K., and Williams, M.C., J. Rheology, 27, 451, 1983.

(3) Valtadoros, T.H., Wong, V.W. and Heywood, J.B., Division of Petroleum Chemistry Preprints, Vol. 36, No. 1, pp 66-78, 1991, Am. Chem. Soc., Atlanta Meeting, April 14-19, 1991.

(4) Trippe, J.C., Hadermann, A.F. and Cole, J.A., US Patent, 5906665, May 25, 1999.

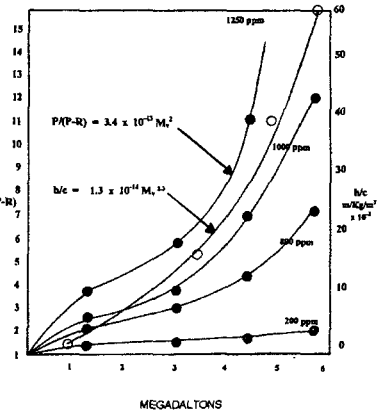

Figure 1. Antimisting function, P/(P-R) and ductless siphon function, h/c vs. molecular weight of polyisobutylene at 20°C (● in diesel fuel, ○ in toluene).

TABLE 1. ENGINE TEMPERATURES OF A 4-CYCLE, SINGLE-CYLINDER GASOLINE ENGINE

	CYLINDER HEAD EXHAUST		
FUEL	RANGE	AVERAGE	DIFFERENCE
No polymer	290-300°F	295°F	
With polymer	260-270°F	265°F	-30°F
	EXHAUST MANIFOLD		
	RANGE	AVERAGE	DIFFERENCE
No polymer	1280-1360°F	1320°F	
With polymer	1208-1248°F	1228°F	-92°F
	TAILPIPE		
	RANGE	AVERAGE	DIFFERENCE
No polymer	980-1110°F	1045°F	
With polymer	798-862°F	830°F	-215°F

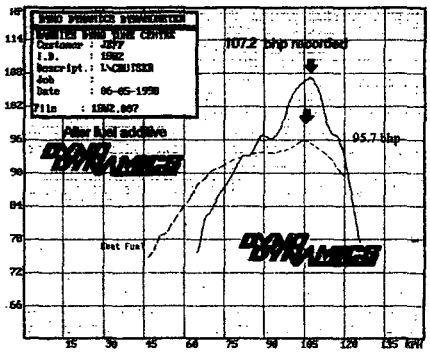

Figure 2. Brake horsepower (BHP) of a 1990 turbodiesel Toyota Landcruiser with polymer (solid line) and without polymer (broken line).

TABLE 2. VEHICLE EMISSIONS TEST RESULTS

		HC			CO			NOx		
Vehicle	Test	BEFORE (PPM)	AFTER (PPM)	LOSS %	BEFORE %	AFTER %	LOSS %	BEFORE (PPM)	AFTER (PPM)	LOSS %
'97 Jeep Wrangler	Sun Dyno	22	6	72	0.02	0.0	100	34	0.0	100
'95 Nissan Pathfinder	"	92	8	91	0.10	0.0	100	162	0.0	100
'88 Chevy Suburban	"	139	54	61	0.32	0.05	84	370	151	59
'90 Ford Bronco	Bear Static	135	0.0	100	0.90	0.0	100	not measured		
'87 Toyota Pickup	"	280	40	86	1.50	0.0	100	not measured		

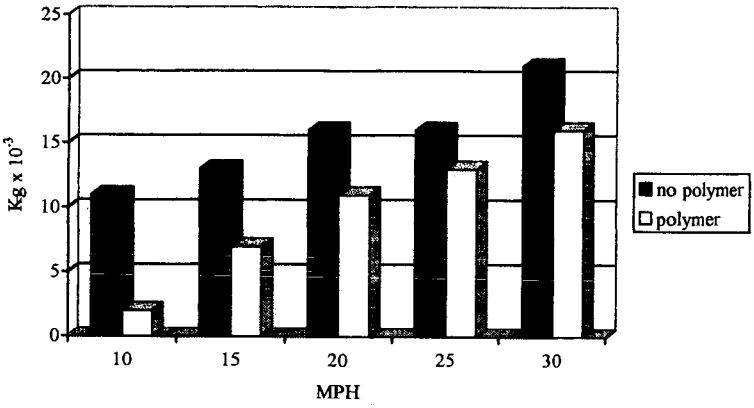

Figure 3. Acceleration tests on a 1987 gasoline-powered Nissan 300 ZX.

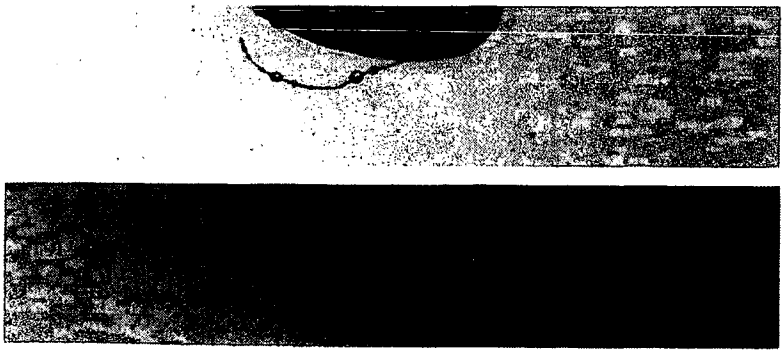

Figure 4. Laser light scattering images of droplets of an aqueous solution of polyethylene oxide (low density) and water (high density)

CARBON NUMBER CORRELATION OF OVERALL RATE CONSTANT OF PYROLYSIS OF N-ALKANES

Masaru Watanabe, Tadafumi Adschiri, and Kunio Arai
Department of Chemical Engineering, Faculty of Engineering, Tohoku University
07, Aramaki, Aoba, Sendai, 980-8579, JAPAN

KEYWORDS: n-alkane pyrolysis, kinetic model, size dependence

Introduction

A lot of studies have been reported so far on pyrolysis of n-alkanes. From the literature, the overall rate constant of pyrolysis of n-alkanes is well known to affect on reaction condition (pressure and temperature) and carbon number of n-alkane.

The pressure dependence of reaction rate can be predicted by Rice and Herzefeld theory[1]. However, carbon number dependence of overall rate constant of n-alkane has not been explained by theoretical base, yet.

For carbon number dependence of the overall pyrolysis rate constant, two correlations were reported[2,3]. Voge and Good's correlation[3] is as:

$$k_{(i)}\ [s^{-1}] = (i-1)\ (1.57i - 3.9) \times 10^{-5} \qquad (1)$$

Herein, $k[s^{-1}]$ is the pseudo first order rate constant of pyrolysis of n-alkanes and i is carbon number of n-alkane. This equation can be applied for the pyrolysis of n-C_4 ~ n-C_{16} at 773 K and 0.1 MPa. Tilicheev's correlation[2] obtained for n-C_{12} ~ n-C_{32} at 698 K and 15 MPa has a different function of i.

$$k_{(i)}\ [s^{-1}] = (2.3i - 15.6) \times 10^{-5} \qquad (2)$$

On the other hand, Yu and Eser[4] proposed the normalized expression of the overall rate constant of n-alkanes (n-C_8 ~ n-C_{16}) using the overall rate constant of n-dodecane (n-C_{12}) at 698 K and a reaction pressure (0.1 MPa ~ 15 MPa) recently, as follows

$$k_{(i)} / k_{12} = (1.89i - 12.3) \times 10^{-1}, \qquad (3)$$

where k_{12} is the overall rate constant of n-C_{12} pyrolysis at 698 K and a given pressure. This equation suggests that the carbon number dependence of the overall rate constant of n-alkane pyrolysis can be expressed by the same function for carbon number regardless of the reaction temperature and pressure (concentration).

A motivation of this study was to give a reasonable explanations for the above three correlations on the theoretical basis, and to proposed a global model for the pyrolysis of n-alkanes. In this study, we proposed the global model for pyrolysis of n-alkanes (n-C_3 ~ n-C_{32}) in a wide range of reaction conditions (572 K ~ 973 K, 6.86×10^{-3} M ~ 2.72 M). Next, we explain previously reported size dependence[2,3,4], based on the proposed model.

Model

The model is considered the following five elementary reaction groups: 1) initiation: a reaction of a C-C bond cleavage of n-C_i, 2) isomerization: an odd electron position in an alkyl radical through intra- and intermolecular H abstraction, 3) β-scission: a reaction of an alkyl radical decomposition, 4) H abstraction: a reaction of an odd electron transfer between n-C_i and an alkyl radical, 5) termination: a reaction of recombination of two alkyl radicals. Applying steady-state approximation for concentration of alkyl radical and considering the carbon number size dependence for the rate constants of bimolecular reactions (details in elsewhere[5]), the apparent first order rate constant of n-C_i pyrolysis can be expressed as

$$k_{(i)} = \frac{k_{\beta(i)} k_{H(i)} \sqrt{\frac{2k_{init(i)}[n-C_i]}{k_{term0}}}}{k_{\beta(i)} + (1/i)k_{H(i)}[n-C_i]}, \quad (4)$$

where $k_{\beta(i)}$ is the rate constant of β-scission of a radical (R_i), $k_{H(i)}$ is the rate constant of H abstraction of an alkyl radical from n-C_i, $k_{init(i)}$ is the rate constant of C-C bond cleavage of n-C_i, and k_{term0} is the rate constant of recombination of two methyl radicals. In the following, the method to evaluate each elementary reaction rate constant is shown.

1) Initiation

In the model, initiation occurs only for mother n-alkanes (n-C_i), because amount of n-C_i is much more than that of the other species at a lower conversion level. We took into account of the number of C-C bond for the overall rate constant of initiation since the rate constant of C-C bond rupture of n-C_i is assumed to be the same for any n-alkane. The activation energy of the rate constant of initiation with forming methyl radical ($k_{init(M)}$) should be 13 kJ/mol higher than that of forming the other radicals ($k_{init(O)}$)[6]. The frequency factor is the same for $k_{init(M)}$ and $k_{init(O)}$ as to be A_{init}[7]. Therefore, the overall rate constant of initiation of n-C_i, $k_{init(i)}$, should be as

$$k_{init(i)} = 2k_{init(M)} + (i-3)k_{init(O)} = A_{init} \exp\left(-\frac{E_{init}}{RT}\right)\left\{2\exp\left(-\frac{16.7\ kJ/mol}{RT}\right) + (i-3)\right\}, \quad (5)$$

where A_{init} is $10^{18.7}$ h^{-1} and E_{init} is 343 kJ/mol, which is C-C bond energy between two secondary carbons for n-butane[6,7].

2) Isomerization

Isomerization is an intramolecular H abstraction. Although this rate constant is not used in Eq. 4, this reaction is essential to determine the rate constant of β-scission, $k_{\beta(i)}$. An odd electron position on an alkyl radical is evaluated statistically, because the rate of isomerization is much faster than that of the other propagation reaction. The activation energy of rate constant of intra- and inter-molecular H abstraction from primary carbon ($k_{H(P)}$) is 16.7 kJ/mol higher than that from secondary carbon ($k_{H(S)}$)[8,9], and the frequency factor of both $k_{H(P)}$ and $k_{H(S)}$ is the same[8,9].

Isomerization of R_i produces as primary radicals, R_i^1 and R_i^i, or secondary radicals, R_i^j ($2 \le j \le i-1$). There are six possible positions on two primary carbons for an odd electron, since each of two primary carbons has three hydrogens. There are $2 \times (i-2)$ possible positions on (i–2) secondary carbons, since each of (i–2) secondary carbons has two hydrogens. Therefore, the probability of an odd electron on a primary carbon in R_i (R_i^1 or R_i^i), $P_{(Pi)}$, can be expressed as

$$P_{(Si)} = \frac{6k_{H(P)}}{6k_{H(P)} + 2(i-2)k_{H(S)}} = \frac{6\frac{k_{H(P)}}{k_{H(S)}}}{6\frac{k_{H(P)}}{k_{H(S)}} + 2(i-2)} = \frac{6\exp\left(\frac{-16.7kJ/mol}{RT}\right)}{6\exp\left(\frac{-16.7kJ/mol}{RT}\right) + 2(i-2)}. \quad (6)$$

The probability of an odd electron on a secondary carbon (R_i^j) ($2 \le j \le i-1$), $P_{(Si)}$, is as

$$P_{(Si)} = \frac{2(i-2)k_{H(S)}}{6k_{H(P)} + 2(i-2)k_{H(S)}} = \frac{2(i-2)}{6\frac{k_{H(P)}}{k_{H(S)}} + 2(i-2)} = \frac{2(i-2)}{6\exp\left(\frac{-16.7kJ/mol}{RT}\right) + 2(i-2)}. \quad (7)$$

3) β-scission

The activation energy of the rate constants of β-scission of forming methyl radical ($k_{\beta(M)}$) is 8.4 kJ/mol higher than that for forming the other radicals ($k_{\beta(O)}$)[9] and both frequency factors of the rate constants of β-scission forming methyl radical ($k_{\beta(M)}$) and that for forming the other alkyl radicals ($k_{\beta(O)}$) are the same[7]. Here, we took into account of the number of C-C bond for the overall rate constant of β-scission.

The primary radical (R_i^1 or R_i^i), which has an odd electron on a primary carbon, has one β-position and produces ethylene and R_{i-2} through β-scission. Since the probability of the

formation of R_i^1 or R_i^i through isomerization is $P_{(Pi)}$, the rate of the formation of ethylene and R_{i-2} through β-scission from R_i is $P_{(Pi)}k_{\beta(O)}[R_i]$. For the secondary radical that has an odd electron at 2 or i-1 position in the radical (R_i^2 or R_i^{i-1}), there is one β-position in the molecule and the radical produces propylene and R_{i-3} through β-scission. The probability of j =2 or i-1 for R_i^j is $2P_{(Si)}/(i-2)$ because there are two carbons corresponding to the position of j = 2 or i-1 in i-2 secondary carbons. Thus, the formation rate of propylene and R_{i-3} through β-scission from R_i is $2P_{(Si)}/(i-2)\ k_{\beta(O)}[R_i]$. In the case of R_i^3 or R_i^{i-2}, there are two β-positions in the radical. From the one of the ways of β-scission of R_i^3 or R_i^{i-2}, methyl radical and 1-alkene has i-1 carbon (Ol_{i-1}) are produced. From the another way, butylene (Ol_4) and R_{i-3} are formed. In i-2 secondary carbons, there are two position corresponding to j = 3 or i-2. Thus, the formation rates of methyl radical and Ol_{i-1} and that of Ol_4 and R_{i-3} are $2P_{(Si)}/(i-2)\ k_{\beta(M)}[R_i]$ and $2P_{(Si)}/(i-2)\ k_{\beta(O)}[R_i]$, respectively. For the case of $4 \le j \le i-3$ of R_i^j, there are also two β-positions in the radical. The β-scission of R_i^j produces Ol_{j+1} and $R_{i-(j+1)}$ from one of the two ways and $Ol_{i-(j-2)}$ and R_{j-2} from the other. The formation rate of Ol_{j+1} and $R_{i-(j+1)}$ or $Ol_{i-(j-2)}$ and R_{j-2} from R_i^j through β-scission is thus $2(i-6)P_{(Si)}/(i-2)\ k_{\beta(O)}[R_i]$ because there are i-6 carbons that are $4 \le j \le i-3$ in R_i^j. The overall rate constant of disappearance of R_i through β-scission ($k_{\beta(i)}$) should be as follows since that rate is the summation of the above formation rate constant of 1-alkenes and alkyl radicals;

$$k_{\beta(i)} = P_{(Mi)}k_{\beta(O)} + \frac{2P_{(Si)}}{i-2}k_{\beta(O)} + \frac{2P_{(Si)}}{i-2}k_{\beta(M)} + \frac{2P_{(Si)}}{i-2}k_{\beta(O)} + \frac{2(i-6)P_{(Si)}}{i-2}k_{\beta(O)}. \qquad (8)$$

From Eqs. (6) and (7), Eq. (8) is as

$$k_{\beta(i)} = A_\beta \exp\left(-\frac{E_\beta}{RT}\right)\left\{\frac{4\exp\left(-\frac{8.4\ kJ/mol}{RT}\right)}{6\exp\left(-\frac{16.7\ kJ/mol}{RT}\right)+2(i-2)} + \frac{6\exp\left(-\frac{16.7\ kJ/mol}{RT}\right)+4(i-4)}{6\exp\left(-\frac{16.7\ kJ/mol}{RT}\right)+2(i-2)}\right\}, \qquad (9)$$

where A_β and E_β are the kinetic parameters of β-scission for R_4^1 producing Ol_2 and R_2 and $10^{15.9}$ h^{-1} and 100.4 kJ/mol, respectively[10].

4) H abstraction

In this model, H abstraction occurs only for n-C_i because n-C_i is the most abundant in the system at a low conversion level. The activation energy of rate constant of H abstraction from primary carbon ($k_{H(P)}$) is 16.7 kJ/mol higher than that from secondary carbon ($k_{H(S)}$)[8, 9], and the frequency factor of both $k_{H(P)}$ and $k_{H(S)}$ is the same. Thus, $k_{H(i)}$ is defined as below because n-C_i has 6 primary hydrogens and 2(i-2) secondary hydrogens:

$$k_{H(i)} = 6k_{H(P)} + 2(i-2)k_{H(S)} = 2A_H \exp\left(-\frac{E_H}{RT}\right)\left\{3\exp\left(-\frac{16.7\ kJ/mol}{RT}\right)+(i-2)\right\}, \qquad (10)$$

where A_H and E_H are the kinetic parameters of H abstraction of methyl radical from a secondary carbon from n-propane and 10^{12} $M^{-1}h^{-1}$ and 42.5 kJ/mol, respectively[11]. In the recent study[5], we found that the rate of H abstraction for n-C_{16} by R_j can be expressed as $(1/j)k_{H(16)}[R_j][n\text{-}C_{16}]$. The radical size dependence of H abstraction is reasonable both from the collision theory and transition-state theory[5]. Thus, for n-C_i, the H abstraction rate for n-C_i by R_j can be described as $1/j\ k_{H(i)}[R_j][n\text{-}C_i]$.

5) Termination

Since a contribution of disproportion between two alkyl radicals is negligible[11], the radical reaction network of n-C_i pyrolysis is terminated by only the recombination of two radicals. With the analogy of H abstraction, the rate constant of termination between R_i and R_m is assumed to be expressed by $(1/i)(1/m)k_{term0}$, where k_{term0} is the intrinsic rate constant and k_{term0} reported for two methyl radicals is employed ($A_{term} = 10^{14.3}$ $M^{-1}h^{-1}$ and $E_{term} = 0$ kJ/mol)[11].

Results and Discussion

1. Comparison between experimental results and calculated results

Figure 1 shows the parity plot between the experimental results and the model. In the case the experiments were conducted using flow type apparatus, the concentration was estimation from the reaction pressure and temperature by Peng-Robinson equation of state[12]. The critical constants (T_c, P_c, and ω) were from the book by Reid et al.[13] or calculated by the ABC method[14]. As shown in Fig. 1, the model described the experimental results successfully over a wide range of experimental conditions (T = 572 K ~ 973 K, $[n\text{-}C_i] = 6.86 \times 10^{-3}$ M ~ 2.72 M, and i = 3~32).

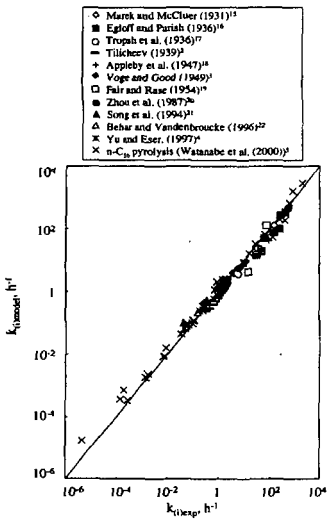

Figure 1 Parity plot of overall rate constants of n-alkanes pyrolysis

2. Correlation of the overall rate constant with carbon number of n-alkane

The rate constant of initiation (Eq. 4) can be approximated as follows because $k_{init(M)}$ is much less than $k_{init(O)}$:

$$k_{init(i)} \approx (i-3)k_{init(O)}. \tag{11}$$

From Eq. 9, the rate constant of β-scission at a long chain n-alkane (i ›› 4) can be simplified to

$$k_{\beta(i)} \approx \frac{4(i-4)}{2(i-2)} k_{\beta(O)} \approx 2k_{\beta(O)}, \tag{12}$$

since $k_{\beta(M)}$ is much less than $k_{\beta(O)}$ and $P_{(Mi)}$ is much less than $P_{(Si)}$. The rate constant of H abstraction (Eq. 10) can be simplified as

$$k_{H(i)} \approx 2(i-2)k_{H(S)}, \tag{13}$$

because the contribution of $k_{H(P)}$ to $k_{H(i)}$ is much less than that of $k_{H(S)}$. Thus, using the approximation of Eqs. 11 ~ 13, Eq. 4 can be approximated by

$$k_{(i)} \approx \frac{2k_{\beta(O)} \cdot 2(i-2)k_{H(S)}}{2k_{\beta(O)} + (1/i) \cdot 2(i-2)k_{H(S)}[n-C_i]} \sqrt{\frac{2(i-3)k_{init(O)}[n-C_i]}{k_{term0}}}. \tag{14}$$

When i is much larger than 2, i-2/i is almost equal to unity. Thus, Eq. 14 becomes

$$k_{(i)} \approx \frac{2k_{\beta(O)} \cdot 2(i-2)k_{H(S)}}{2k_{\beta(O)} + k_{H(S)}[n-C_i]} \sqrt{\frac{2(i-3)k_{init(O)}[n-C_i]}{k_{term0}}} = (i-2)\sqrt{i-3}\left\{\frac{4k_{\beta(O)}k_{H(S)}}{2k_{\beta(O)} + k_{H(S)}[n-C_i]} \sqrt{\frac{2k_{init(O)}[n-C_i]}{k_{term0}}}\right\} \tag{15}$$

Therefore, regardless to the temperature and concentration, the overall rate constant of n-alkane pyrolysis depends on $(i-2)\sqrt{i-3}$ for carbon number of n-alkane. Normalizing the rate constant of n-alkane pyrolysis by the rate constant of n-C_{16} pyrolysis at a given condition, Eq. 15 is as

$$\frac{k_{(i)}}{k_{(16)}} = \frac{(i-2)\sqrt{i-3}}{14\sqrt{13}}. \tag{16}$$

Figure 2 shows the normalized rate by Eq. 19.Tilicheev's[2], Voge and Good's[3], and Yu and Eser's[4] correlations with Eqs. 1, 2, and 3, respectively, are also shown in this figures. As shown in Fig. 2, all the plots by Tilicheev's[2], Voge and Good's[3], and Yu and Eser's[4] correlations fall on the line calculated by Eq. 16. This analysis gives the theoretical basis to their correlations.

Conclusion

We proposed a new model for overall rate constant of n-alkane pyrolysis, based on Kossiakoff and Rice theory, by taking the carbon number dependence of alkyl radical for the rate constant of bimolecular reactions into account. The model can express the experimental overall rate constant of n-alkanes (n-C_3 ~ n-C_{32}) at wide range of temperatures (572 K ~ 973 K) and concentrations (6.86×10^{-3} M ~ 2.72 M), and could explain previously reported carbon number correlation of pyrolysis rate.

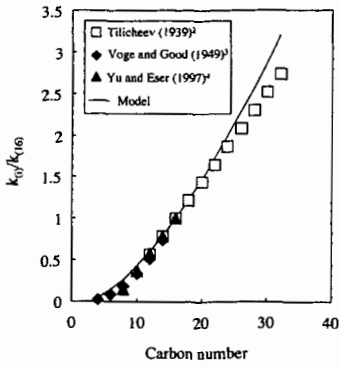

Figure 2 Normalization of carbon number dependence of Voge and Good's[3], Tilicheev's[2], and Yu and Eser's[4] correlation by the overall rate constant of n-C_{16} pyrolysis at given conditions

Acknowledgement

The authors wish to acknowledge the Ministry of Education, Science, Sports and Culture, Japan and New Energy and Industrial Technology Organization (NEDO) for financial support of this research.

Literature Cited

(1) Rice, F. O.; Herzefeld, K. F., *J. Am. Chem. Soc.* **1934**, *56*, 284-289.

(2) Tilicheev, M. D., *Foreign Petrol. Technol.* **1939**, *7*, 209-224.

(3) Voge, H. H.; Good, G. M.,. *J. Am. Chem. Soc.* **1949**, *71*, 593-597.

(4) Yu, J.; Eser, S., *Ind. Eng. Chem. Res.* **1997**, *36*, 585-591.

(5) Watanabe, M.; Tsukagoshi, M.; Hirakoso, H.; Adschiri, T.; Arai, K.,.*AIChE J.* **2000**, *46*, 843-856.

(6) Benson, S. W. *Thermochemical Kinetics, 2nd edition*; Wiley: New York, 1976.

(7) Nigam, A.; Klein, M. T., *Ind. Eng. Chem. Res.* **1993**, *32*, 1297-1303.

(8) Fabuss, B. M.; Smith, J. O.; Satterfield, C. N., *Adv. Pet. Chem. Refin.* **1964**, *9*, 157-201.

(9) Murata, M.; Saito, S.; Amano, A.; Maeda, S., *J. Chem. Eng. Jpn.* **1973**, *6*, 252-258.

(10) Doue, F.; Guiochon, G., *J. Chim. Phys.* **1968**, *65*, 395-409.

(11) Allara, D. L.; Shaw, R., *J. Phys. Chem. Ref. Data* **1980**, *9*, 523-559.

(12) Peng, D. Y.; Robinson, D. B., *Ind. Eng. Chem. Fundam.* **1976**, *15*, 59-68.

(13) Reid, R. C.; Prausnitz, J. M.; Sherwood, T. K. *The Properties of Gases and Liquids, 3rd edition*; McGraw-Hill: New York, 1977.

(14) Marano, J. J.; Holder, D., *Ind. Eng. Chem. Res.* **1997**, *36*, 1895-1907.

(15) Merek, L. F.; McCluer, W. B. *Ind. Eng. Chem.* **1931**, *23*, 878.

(16) Egloff, G.; Parrish, C. I., *Chem. Rev.* **1936**, *19*, 145-161.

(17) Tropsch, H.; Thomas, C. L.; Egloff, G., *Ind. Eng. Chem.* **1936**, *28*, 324-332.

(18) Appleby, W. G.; Avery, W. H.; Meerbott, W. K. *J. Am. Chem. Soc.* **1947**, *69*, 2279.

(19) Fair, J. R.; Rase, H. F. *Chem. Eng. Progr.* **1954**, *50*, 415.

(20) Zhou, P.; Hollis, O. L.; Crynes, B. L., *Ind. Eng. Chem. Res.* **1987**, *26*, 846-582.

(21) Song, C.; Lai, W.; Schobert, H. H., *Ind. Eng. Chem. Res.* **1994**, *33*, 548-557.

(22) Behar, F.; Vandenbroucke, M., *Energy & Fuels* **1996**, *10*, 932-940.

PREPARATION AND CHARACTERIZATION OF Co-Mo/SiO_2-Al_2O_3 CATALYSTS

Shakeel Ahmed[1] Mazen A Shalabi[2]
[1]The Research Institute, King Fahd University of Petroleum and Minerals,
Dhahran 31261, Saudi Arabia
[2]Department of Chemical Engineering

KEYWORDS: Hydrocracking catalysts, TPR/TPS/TPD, HDS

INTRODUCTION

Hydrocracking catalysts are bifunctional catalysts having both hydrogenation-dehydrogenation function and an acidic function. Proper balancing of the two functions plays a prominent role in deciding the performance of the catalyst for application in hydrocracking [1]. The cracking function is provided by an acidic support, whereas the hydrogenation-dehydrogenation function is provided by metals. The acidic support consists of (a) amorphous oxides (e.g., silica-alumina), (b) a crystalline zeolite (mostly modified Y zeolite) plus binder (e.g., alumina), or (c) a mixture of crystalline zeolite and amorphous oxides. Cracking and isomerization reactions take place on the acidic support. The metals providing the hydrogenation-dehydrogenation function can be noble metals (palladium, platinum) or non-noble metal sulfides from group VIA (molybdenum, tungsten) and group VIIIA (cobalt, nickel). These metals catalyze the hydrogenation of the feedstock, making it more reactive for cracking and heteroatom removal, as well as reducing the coking rate. They also initiate the cracking by forming a reactive olefin intermediate via dehydrogenation. The ratio between the catalyst's cracking function and hydrogenation function can be adjusted to optimize activity and selectivity. For a hydrocracking catalyst to be effective, it is important that there be a rapid molecular transfer between the acid site and hydrogenation sites in order to avoid undesirable secondary reactions. Rapid molecular transfer can be achieved by having the hydrogenation sites located in the proximity of the cracking (acid) sites [2]. Catalysts with amorphous support are in commercial use, primarily where maximizing the production of middle distillates or conversion to lube oil blending stock is the objective [3,4]. Amorphous hydrocracking catalysts contain primarily amorphous silica-alumina [5]. Other amorphous supports reported are titania-zirconia, silica-alumina dispersed in alumina, alumina-boria, and other acidic mixed oxides. Hydrocracking catalysts containing fluorinated inorganic oxides as supports have also been reported [6]. In this research work a series of CoMo-silica-alumina amorphous base hydrocracking catalysts was prepared by impregnation method. The amorphous silica alumina support was prepared in the laboratory by co-precipitation method. The effect of order of impregnation of cobalt and molybdenum on the catalyst activity was studied by specific characterization methods and model compounds reactions. In addition, γ-alumina and Y-zeolite based catalysts were also prepared and studied for comparison purposes.

EXPERIMENTAL

Catalyst Preparation: A series of silica-alumina supported CoMo hydrocracking catalysts were prepared by impregnation method. The order of impregnation of cobalt and molybdenum was varied. For catalyst HC-1, molybdenum was impregnated first and then cobalt was loaded. In catalyst HC-2, this order was reversed. On the other hand, simultaneous impregnation of cobalt and molybdenum was adopted for the preparation of catalyst HC-3. All catalysts were calcined at 500 °C for three hours in a stream of dry air. The silica-alumina supports were also prepared in the laboratory by co-precipitation method. In addition, γ-alumina and 50% mixture of γ-alumina and commercial Y-zeolite were also used as supports. Catalyst HC-4 was prepared by using commercial acidic alumina supplied by Aldrich. For the preparation of catalyst HC-5, a 50% mixture of commercial γ-alumina (Aluminum Company of America) and Y-zeolite (CATAL, UK) was used. Commercial γ-alumina and Y-zeolite were dried at 250 °C before using as catalyst support.

Catalyst Characterization: The catalysts samples were characterized by temperature-programmed desorption (TPD) of ammonia, temperature-programmed reduction (TPR), and temperature-programmed sulfiding (TPS). The details of the measurements are given elsewhere [7]. The elemental composition of the catalysts was measured by ICP. Surface area (BET method) and pore volume was measured by Quantachrome (NOVA 2000).

Catalyst Evaluation: The prepared hydrocracking catalysts were evaluated for HDS and cracking activities using thiophene and cumene as model compounds, respectively. The activity measurements were conducted in a pulse type micro reactor. The detailed experimental procedures are given elsewhere [7].

RESULTS AND DISCUSSION

Some of the physico-chemical properties of the prepared catalysts are given in Table 1. It was observed that the surface area of the catalyst was reduced as compared with the blank support, after the impregnation of the metals. This could be due the pore blocking by cobalt and molybdenum in the catalysts. This was also evident from the reduction in pore volume of the catalysts in comparison with the respective support. However, the reduction in surface area for

the γ-alumina-based catalyst (HC-4) was not as pronounced as in the case of synthesized silica-alumina-based catalysts. Similarly, the surface area of HC-5 was comparable with the average surface area of the respective support.

Temperature-Programmed Reduction: The results of temperature-programmed reduction of silica alumina and zeolite based catalysts are given in Figure 1. Almost all the catalysts show a multiple peak reduction behavior. The first reduction appear in the region of 300 to 500 °C. The variation in the peak temperature was attributed to the differences in the metal support-interactions and multiple peak pattern might be due to the presence of molybdenum at different sites of the support. The highest reduction temperature was observed for HC-1 (peak at 363 °C). On the other hand, HC-5 reduced at minimum temperature in the series giving a shoulder at 397 °C with the main peak at 462 °C. It was also observed that catalyst prepared by simultaneous impregnation of metals (HC-3) reduced at lower temperature (431 °C) as compared with its homologues. The reduction emperature indicates the metal-support interaction, which intern influences the HDS activity of the catalyst.

Temperature-Programmed sulfiding: The results of temperature-programmed sulfiding are given in Figure 2. The TPS profiles are similar to the molybdenum containing commercial catalysts. The upper curve represents the UV-detector signal, which monitors the hydrogen sulfide concentration, where the positive peak means the production of hydrogen sulfide and the negative peak means consumption. The lower curve is a response of the TCD, which monitors the hydrogen concentration, and the positive peak in this case indicates the consumption of hydrogen. The TPS profile can be divided into four regions. In the region I (25 to <100 °C) the positive peak in UV signal is due to the desorption of hydrogen sulfide, which was mainly adsorbed physically during stabilization at room temperature. The desorption of hydrogen sulfide is followed by a low-temperature sulfiding in region-II (below 200 °C). No hydrogen is consumed in this region as noticed in the lower curve. Arnoldy et al. [8] showed in their study that sulfiding in this region occurs by simple O-S exchanges on Mo^{+6}. In region-III, hydrogen sulfide is produced as a sharp peak, coupled with the consumption of hydrogen. The sharpness of the peak points to a chemically well-defined surface compound. In this region Mo^{+6}-S bond is breaking down and the free sulfur is reduced so the hydrogen sulfide is produced. This peak appeared at 134 °C for HC-5 whereas, for HC-2 it is at 218 °C. The sharpness of the peak in catalyst HC-2 also indicates the homogeneous distribution of molybdenum over the catalyst support. Note that in this sample, molybdenum was impregnated after the cobalt loading. While, catalyst HC-1 gave relatively broad peak at 199 °C in which the order of impregnation was reversed. This gives some indication that there may exists some competition between the metal ions being impregnated over the support. High temperature sulfiding (region-IV) is taking place above 250°C in all cases. In this region, most of Mo ions are already in Mo^{+4} state, sulfiding can be described mainly as O-S exchange on Mo^{+4} ions. Sulfiding appears to be completed at about 800°C in all cases. In this region, HC-4 gave a shallow peak as compared to other catalysts. On the other hand, HC-2 and HC-3 showed maximum consumption of H_2S in this region.

Temperature-programmed Desorption: Total acidity of the silica alumina and zeolite based catalysts, measured by TPD of ammonia is given in the Table 2. Figure 3 shows the TPD curves of these catalysts. The total acidity (Bronsted and Lewis) measured was in the range of 0.3 to 0.8 m mole/g. For the catalysts HC-1, -2 and -3 the order of impregnation of cobalt and molybdenum appears to be playing a role in determining the acidity. It was found to be highest in the case of simultaneous impregnation of the metals. Quite interestingly, the total acidity was lower for the catalyst containing Y-zeolite (HC-5) as compared with some of the silica-alumina based catalysts. This indicates that there might be more Lewis acid sites in silica-alumina based catalysts as compared with zeolite containing catalyst. The cracking of cumene will give more information about the acidic properties of the catalysts.

Catalytic Activity: Hydrocracking of cumene was performed to evaluate the cracking property of the catalysts. The results of cumene cracking are given in Figure 4. Maximum cracking activity was observed for HC-5 (zeolite based). This higher cracking activity was attributed to the presence of Y-zeolite in the catalyst. HC-3 catalyst showed maximum total acidity (0.765 m mol/g), but it gave lower cumene cracking (46.7%) as compared to HC-5 (97.9% cumene conversion). It was observed that total acidity measured by TPD of ammonia was not well correlating with the cracking of cumene. This indicates that Lewis acid sites are contributing more to the acidity measurement as compared to the Bronsted acidity (for silica-alumna catalysts) which is required for cracking activity. In the silica-alumina based catalyst series, maximum cumene cracking was found for HC-1 (78.5%) whereas, HC-2 gave minimum conversion (34.3%). This shows that the order of impregnation of cobalt and molybdenum plays an important role in the cracking activity of cumene. The cracking activity was higher when molybdenum was impregnated first and lower in the case where cobalt was impregnated first followed by molybdenum. Total acidity was also lower for HC-2 as compared with that of HC-1. These results show that cobalt is interacting with the acid sites and blocking them so that

the total acidity was decreased. This requires further investigations in terms of metal-acid-sites interactions.

The hydrodesulfurization of thiophene was performed to measure the HDS activity of the catalysts. Figure 5 shows the results of HDS of thiophene at different temperatures. The highest HDS activity was found in the case of HC-4 (alumina based catalyst). On the other hand, minimum HDS activity was observed for HC-1. Here also the order of impregnation of metals plays a role. In the series of silica-alumina based catalysts, the highest HDS activity was found for HC-3. In the catalyst cobalt and molybdenum were impregnated simultaneously. A trend was observed between the HDS activity and the reduction temperature measured by TPR. It was found that at lower reduction temperature higher HDS activity occurred. Figure 6 shows the correlation of thiophene conversion versus peak temperature of TPR profile. For catalyst HC-5 the average of the two peaks was used for correlation curve.

CONCLUSIONS

The order of impregnation of cobalt and molybdenum over silica-alumina based hydrocracking catalysts plays an important role in terms of catalyst activity. Maximum cracking activity was found for the catalyst prepared by impregnating molybdenum first and then cobalt in the second step over silica-alumina support. Temperature programmed methods were successfully utilized for the characterization of the prepared hydrocracking catalysts. A trend was observed for the HDS activity of the hydrocracking catalysts and reduction temperature measured by TPR method. Catalysts reducing at lower temperature performed better for HDS activity.

ACKNOWLEDGEMENT

The authors wish to acknowledge the support of the Research Institute, King Fahd University of Petroleum and Minerals, and Petroleum Energy Center, Japan, with the subsidy of the Ministry of International Trade and Industry, for this work under KFUPM-RI Project No. 21151.

REFERENCES

[1] Marcilly, C and Frank, J. P., *Stud. Surf. Sci. Cat.*, v. **5**, pp. 93-104 (1980).
[2] Franck, J.P and LePage, J.F., Proc. 7th Intern. Congr. Catal., Tokyo, p.792 (1981).
[3] Bridge, A.G., Jaffe, J., and Powell, B.E., Proc. Mtg. Jap. Petr. Inst., Tokyo, Japan, (1982).
[4] Reno, M.E., Schaefer, B.L., Penning, R.T., and Wood, B.M., NPRA Ann. Mtg. March 1987, San Antonio, TX, AM-87-60.
[5] Sullivan R.F., and Scott, J.W., *Heterogeneous Catalysis: Selected American Histories*, ACS Symposium Series 222, Washington, D.C., p.293 (1983).
[6] Adachi, M., Okazaki, H., and Ushio, M., U.S. Patent No. 4,895,822 (1990).
[7] Ahmed, S., et al., Proceedings of the Sixth Annual Workshop on Catalysts in Petroleum Refining and Petrochemicals, December 1996, pp. 223-234.
[8] Arnoldy, P., Franken. M.C., Scheffer, B., and Moulijin, J.A., *J. Catal.*, v. **92**, pp. 35-55 (1985).

Table 1. Physico-chemical properties of CoMo-supported hydrocracking catalysts

Catalyst Code	Support	Surface Area (m^2/g)	Pore Volume (cm3/g)	CoO (wt %)	MoO_3 (wt %)
HC-1	SA*	145	0.20	3.89	13.2
HC-2	SA	124	0.24	4.86	14.4
HC-3	SA	183	0.19	4.10	15.1
HC-4	γ-Alumina**	140	0.23	5.35	13.7
HC-5	γ-Alumina + Y-Zeolite**	280	0.29	3.74	14.5

* Silica-Alumina support prepared in the laboratory; surface area 376 m^2/g pore volume 0.34 cc/g
** Acidic alumina, surface area 140 m^2/g from Aldrich
** γ-Alumina surface area 216 m^2/g from Aluminum Company of America
Y-Zeolite surface area 515 m^2/g from CATAL, UK.

Table 2. Results of TPD analysis

Catalyst	Acidity (m mol/g)
HC-1	0.589
HC-2	0.288
HC-3	0.765
HC-4	0.320
HC-5	0.413

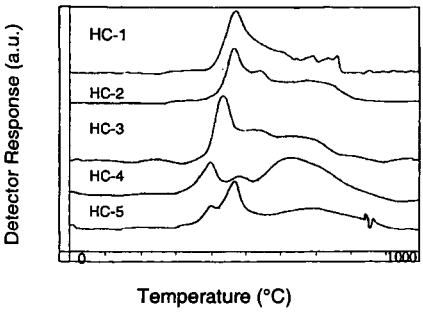

Figure 1. TPR profiles of CoMo-supported hydrocracking catalysts.

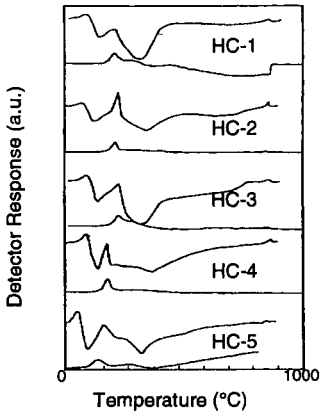

Figure 2. TPS profiles of CoMo-supported hydrocracking catalysts.

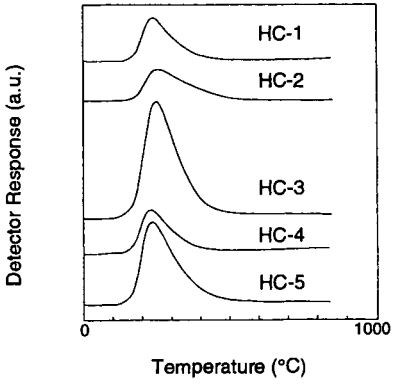

Figure 3. TPD profiles of CoMo-supported hydrocracking catalyst.

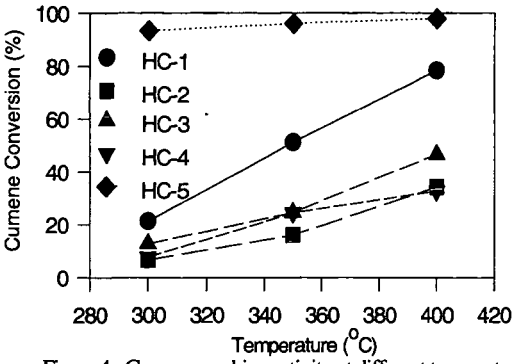

Figure 4. Cumene cracking activity at different temperatures.

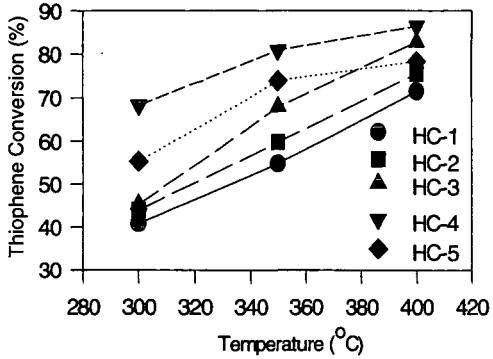

Figure 5. Thiophene HDS activity at different temperatures.

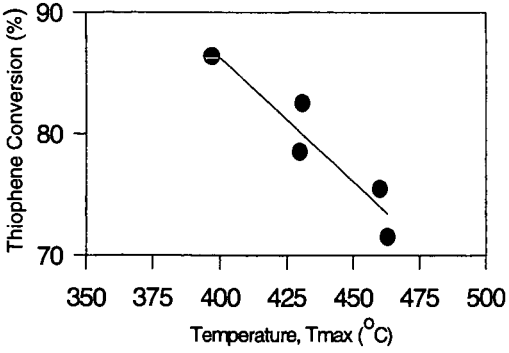

Figure 6. Correlation of thiophene conversion versus TPR Tmax

CONTROL OF SEVERITY IN VISBREAKING

J.A. Carrillo*, F. Pantoja*, G. Garzón*, H. Barrios, J. Fernández**, E. Carmona*** and J. Saavedra*****

*-ECOPETROL-Instituto Colombiano del Petróleo; **-ECOPETROL-Cartagena Management; ***-ECOPETROL- Barrancabermeja Management.

Test results of the behavior of different feeds in the visbreaking process at the pilot as well as the industrial plant level are presented, in agreement with their insoluble matter content in nC_7. The interval studied was 10%m (vacuum barrel bottoms) at 32%m (deasphalted barrel bottoms). In the processing of barrel bottoms, a correlation was found between the abrupt change in the slope of efficiency in function of severity by temperature (at the 745-760 °K interval) regarding the change in slope of the line of stability determined by means of the Merit Test, while at the interval tested for residence time (3.8-6.4 minutes) there was no change in slope found. In the processing of deasphalted barrel bottoms, no correlation was found between the abrupt change in the slope of efficiency in function of the severity by temperature (at the 749-773 °K interval) regarding the change in slope of the line of stability determined by means of the Merit Test, while at the interval of residence time tested (5-13 minutes) a change of slope was found in the Merit Test. In this type of feeds, it was observed that the severity is controlled most efficiently by temperature, without noticeably increasing coke production in the oven, while for barrel bottoms, it is preferred to control severity by means of residence time. The study shows the influence of steam and light cycle oil on the processing of DEMEX barrel bottoms in visbreaking.

In addition, correlations are shown between the Merit Test, the Coking Index using Heithaus and the Stability Factor of the feeds and products.

INTRODUCTION

Visbreaking is a process of thermal breaking of barrel bottoms that is carried out between 748-773 °K, with a residence time (in the reaction zone) of 6-10 minutes. Sometimes from 1 to 4% v of steam and from 0% to 10% of light cycle oil (LCO) is introduced.

Visbreaking is a low capital investment process and is operated at threshold conditions to produce a greater quantity of distillates and reduce the quantity of diluent used in the preparation of fuel oil from visbroken tar. The severity threshold has been studied by several researchers (Savaya, et al., 1988) and it is determined by the stability of the fuel oil and the quantity of coke deposited on the inner walls of the oven. To measure severity in the operation, techniques such as the Merit Test, the Coking Index using Heithaus (John and Adam, 1999) and the Stability Factor (S.F.) which relates oil composition to severity (Kuo, 1984).

Another important factor that limits severity measured in function of conversion is the quality of feed. The greater the quantity of insoluble matter in nC7, greater will the production of barrel bottoms be and the less the production of gas-oil (John and William, 1982).

For this study, only the coil visbreaking technology was considered, because this is the technology of the plants currently operating in ECOPETROL refineries.

EXPERIMENTAL

Simulations at the pilot level were carried out at a plant built in ECOPETROL-Instituto Colombiano del Petróleo (Carrillo and Pantoja, 1998).

The stability of the visbroken residue is determined by means of two tests developed by the IFP (Merit Test) and the WRI (Heithaus Titration Test); which consist of a paper chromatography and the precipitation of asphaltenes with i-octane, and are based on the solubility of the sample to be analyzed in a blend of aromatic and paraffin solvents of known proportions.

For the tests, asphaltenes were obtained from the deasphalted vacuum bottoms of the oil blend of the Barrancabermeja refinery (insoluble matter in n-C7 between 30 and 35%m) and vacuum bottoms of oil blend from the Cartagena refinery whose characteristics are given in Table 1.

Heithaus parameters of severity

Titration using Heithaus consists of taking a constant quantity of a visbroken barrel bottom (2 g) and diluting it in three different volumes of o-xylene: 5, 7 and 9 ml respectively. These concentrations are titrated with isooctane. The methodology is included in Schabron and Pauli.

Table 1: Characteristics of Vacuum Bottoms

Properties/Refinery	Barranca-Bermeja		Cartagena			Standard/equipment
Typo of bottom feed	DEMEX		Vacuum			
nC_7 insolubles, % wt	32.7	30.5	11.9	13.48	16.45	UOP-614
Saturates, % wt	4,0	2,7	11.2	10.8	11.2	Iatroscan Method
Aromatics, % wt	44,4	47,9	56.5	55.9	49.7	Iatroscan Method
Resins, % wt	34,2	33,0	24.1	23.5	28.3	Iatroscan Method
Asphaltene; % wt	17,5	16,4	8.2	9.7	10.8	Iatroscan Method
CCR, % m	38.8	36.5	22.2	22.46	24.53	ASTM D-4530
Merito test	—	3.0	5.0	4	4	IFP
F.E.	0.5	0,8	0.32	0.33	0.28	*
Density @ 15 °C, gr./ cm^3	1.077	1.0892	1.0196	10.254	1.0256	ASTM D-70
Viscosity @ 150 °C, cP			229	421	588	ASTM D-445
VBN	-12,8	-5.2	2.69	1.94	1.03	

* -Calculated by Kuo, 1984. F E = (Aromatics + Resins) / (Saturates * CCR)

Coking index

This index is defined as the peptizabilitation (Pa)/dilution concentration (Cmin) ratio. It is based on the considerations that Pa decreases when the parameter of solubility or the molecular weight of the asphaltenes is increased, and Cmin increases when residue stability decreases. Preliminary studies suggest that a ration near one (1) indicates a highly stable system ratio and coking begins when the ratio is near 0.3.

RESULTS AND DISCUSSION

1. Processing of vacuum barrel bottoms

1.1 Evaluation of severity based on temperature

Product efficiency for the different conditions of severity used, does not vary noticeably for temperatures below 754 °K (figure 1). For temperatures above 754 °K, coke formation is triggered and a drastic reduction in the production of barrel bottoms occurs, which reflects in the increase of gas-oil efficiency (atmospheric + LGO + HGO) and the production of gases and gasoline.

When the content of asphaltenes, resins, coke and some of their correlations are related, similar trends are observed, where the behavior of the asphaltenes that have a maximum of 756 °K stands out, while the resins and the resin/asphaltene ratio shows an opposite behavior. These trends indicate that once the maximum cracking temperature is reached for each feed, the system stops being stable, the miscellar structure is destroyed and the asphaltenes become coke precursors. This instability is confirmed by the Merit Test performed on the visbroken tar, where a change in slope at 754 °K is observed, as is shown in figure 2. At values below this temperature, the visbroken tar is stable, while at higher temperatures the colloidal state is thrown off balance.

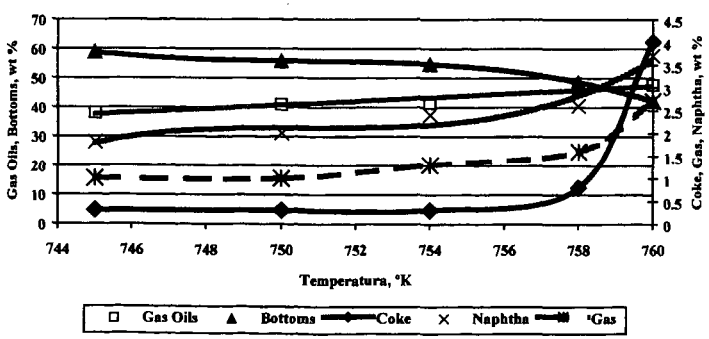

Figure 1. Severity as temperature function

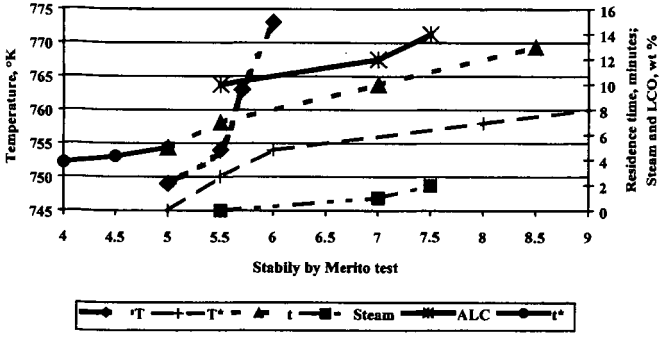

Figure 2. Stability of the visbreaking bottoms by Merite test

1.2 Evaluation of severity based on residence time

At the conditions analyzed there were no abrupt variations in the efficiency of the products. The gases, gasolines, gas-oils and coke are increased in a constant fashion with the increase in residence time, while the production of tar and the resin asphaltene ration is reduced at the same interval analyzed. The resin/asphaltene ratio is greater than that of the data with temperature variation, which explains the greater stability of the visbroken tar. This stability is shown in figure 2, where it is observed that all the values are equal to or below 6 on the Merit Test; in addition there are no changes in slope.

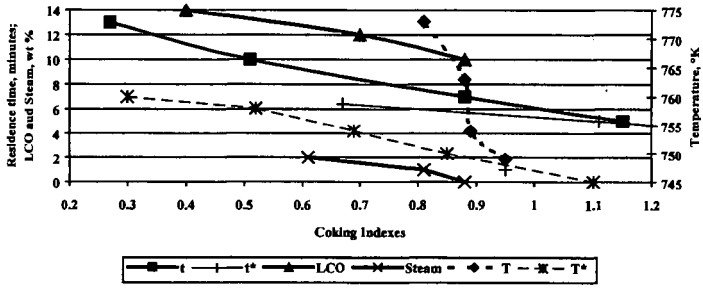

Figure 3. Coking Indexes using The Heithaus Titration and Asphaltene Solubility. Barrancabermeja Refinery

1.3 Correlations between the method of measuring the stability of the visbroken tar by means of Titration using Heithaus with the method based on the Merit Test

Figure 3 presents the titration results for different samples corresponding to variations in severity by residence time and temperature. Similarly, diagrams for steam and light cycle oil were obtained.

When the coking index is illustrated in function of severity by temperature, it is found that the recommended stability interval (0.3 - 1) does not correspond to this type of feed with the results of efficiency (figure 2) and with the Merit Test for the same evaluation. These values indicate that at a temperature of 756°K, there is a transfer from a stable area to an unstable area above this temperature. For this reason, the results seem to indicate that for this type of feed, the control interval to be recommended in the Coking Index should be 0.6-1.

A similar procedure was followed with the samples corresponding to the variation of severity by residence time.

When the modified interval of the Coking Index (0.6-1.0) is the same as in the Merit Test, all the points analyzed are within the stable interval, which supports the fact that the residence time at the interval analyzed shows less risk than the temperature in handling severity.

2. Processing desasphalting bottoms.

2.1 Evaluation of severity based on temperature.

Severity in funtion of temperature was evaluated maintaining residence time constant at 7 min, the LCO at 10% and the amount of steam supplied to the feed in 0%.

In spite of this, the system remains colloidally stable, being that the amount of resins increases and at the same time the asphaltenes decrease, becoming coke as was stated previously. Therefore, all the points analyzed by the Merit Test yield values below 7. This indicates that in the processing of this type of feeds the threshold is not found in the stability of the products, but in the amount of coke deposited on the inner walls of the oven pipes.

2.2 Evaluation of severity based on residence time.

Severity in function of residence time was evaluated keeping temperature constant at 763 °K. This value corresponds to the temperature used at the Barrancabermeja refinery. The LCO percentage was kept at 10%v and the amount of steam supplied to the feed before entering the reactor at 0% v.

Product efficiencies vary noticeably for different conditions of severity used in function of residence time, above all during periods of over seven minutes. With an increase in residence time, the production of gases, gasolines and coke is increased and the production of barrel bottoms is reduced. Just as the influence of the change in severity in function of temperature, it is expected that the increase in severity will increase the production of gas-oils, for which the production of tar would be below that illustrated. With a residence time of 7 minutes, a change is observed in the slope of coke and tar production, which coincides with the change in slope of the stability index as well as residence time. With a residence time of 13 minutes, the system is totally unstable.

The resin/asphaltene ratio shows a slight tendency toward increase as residence time is increased. It would be expected that in this order, the stability of the system increase. Nevertheless, over ten minutes of residence time, the system is unstable possibly due to the abrupt reduction in viscosity or due to the great amount of gas-oil formed in the reaction, which by dilution destabilizes the colloidal system.

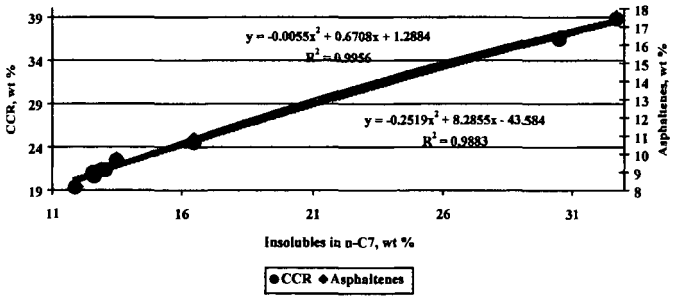

2.3 Severity in function of the percentage of steam.

For these tests, residence time (7 min.), the percentage of LCO (10% V) and temperature (763 °K) are kept constant.

This variable was kept in mind due to the fact that at the Barrancabermeja refinery, the steam is used to reduce the residence time inside the furnace.

It would be expected that by increasing the percentage of steam in the feed, the residence time would be reduced and therefore soften conversion. However, the opposite is observed. When the percentage of steam in the feed is increased, the gasoline production is increased considerably and tar production is reduced drastically. This is due to the fact that the steam helps to decrease the partial pressure of the heavy fragments, improving the distillation process, or perhaps it is a hydrogen donor in the different thermal reactions that take place inside the reactor. Within this explanation, it would be expected for coke production to be reduced, which does not occur in practice, possibly due to a change in the flow rate into two phases. It can also be observed that

the coke has a constant increase with the increase in the amount of steam and that its values are above 1% m, which is a high value and implies rapid oven coking. In spite of the fact that according to the Merit Test (figure 2) the system is within the limits of stability, a change is observed in slope for concentrations above 1% m. The quality of the visbroken tar goes through a process similar to that of the tar coming from the visbreaking of vacuum bottoms as can be seen in figure 4.

2.4 Evaluation of severity in function of the amount of LCO in the feed.

For these tests, residence time (7 min), temperature (763°K) and the amount of steam (0%) were kept constant.

Analyzing the parameters of severity in agreement with the titrations using Heithaus, it is observed that in these tests the temperature has more incidence on the stability of the visbroken star than on residence time.

To apply the corrected value of 6 instead of 0.3 on the stability threshold of Titration using Heithaus we find that the residence times of over 9 minutes give an unstable product which corresponds to two points of the interval analyzed.

In agreement with the Titration using Heithaus, values of over 12% m of LCO in the feed produce instability in the visbroken tar. The stable values in this product in agreement with the Merit Test indicate that up to 14% m of LCO in the feed is allowed. Nevertheless, this same test indicates that there is a change in slope at concentrations of 12% m, which corresponds to a value of 7 on the Merit Test. The point of the change in slope coincides with those registered for the influence of steam and residence time, which indicates that this type of feed should have not 7.5 but 7 as a control of stability on the Merit Test.

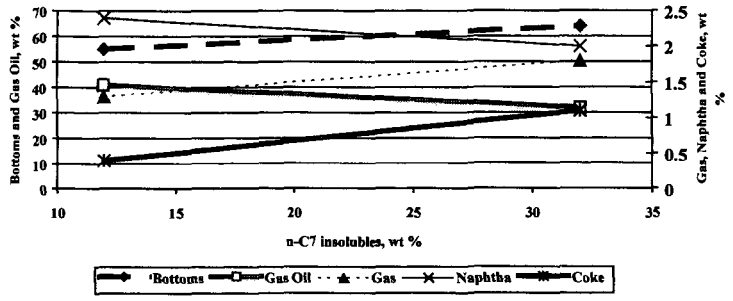

The crackability of feeds is a function of the amount of asphaltenes in it, expressed by means of the amount insoluble in C5 or C7. As this amount increases, the conversion decreases.

CONCLUSIONS

- The most important characteristic defined by cracking of a feed in visbreaking is the amount of asphaltenes it has. The higher the concentration of asphaltenes in the feed, the lower the crackability.

- For DEMEX barrel bottoms, in which the insoluble matter in nC7 are greater than 18% m, the variable that influences operational control most is temperature, which allows increases of up to 758°K reducing the production of visbroken tar by almost 4% m, the ΔVBN increases by 0.3 points and the coke increases by 22% m. At these conditions, the °API remains constant.

- With this same type of feeds, the steam as well as the ALC show similar behavior. It is recommended to use steam between 0.4 and 0.6%m, which means a reduction in tar production by 1% m and in increase in ΔVBN by 1 point and the °API by 0.4 points. Coke production is increased by 16%m. Above 0.6% m of steam, coke production can put the duration of the run at risk due to oven fouling.

- The ALC has a marked influence on the operation, which is why stricter control is recommended.

- For vacuum barrel bottoms, with concentrations of insoluble matter in nC7 below 18% m, the variable that allows the most control of severity is residence time, while for feeds with asphaltene concentrations of over 18% m, the variable that allows better control is temperature.

- The Merit Test as well as the Coking Index characterize visbreaking results well from the visbroken tar stability viewpoint, but not for the oven fouling, especially for feeds with over 18% m insoluble matter in nC7. Nevertheless, the Coking Index is more exact, which is why it is presented as a better tool for operational control.

Literature Cited:

CarrilloJ.A., Pantoja F., Barrios H., Estrada C., Alvarez N. And Chinchilla M. 1999. "Pressure control in vacuum towers". CT&F, Vol. 1 Núm. 5:25-34.

Savaya Z. F., Al-Soufi H.H., Al-Azawi I and Mohamed H.K. 1988. "The effect of Visbreaking conditions on the stability of some Iraqui Long Residues". Fuel Science and Technology INT'L., 6(3):354-366.

Maketta, Jhon and Cunnigham, William, 1982. "Encyclopedia of chemical processing and design", Ney York, Marcel Dekker

Kuo, C, J., 1984. "Effect of crude types on Visbreaking conversion". Oil & Gas Journal (Sept24):100-102.

Schabron J.F and Pauli A.T. 1999. "Coking Index using The Heithaus Titration and Asphaltene Solubility". American Chemical Society, National meeting and exposition program, Anaheim, C.A. (March 21-25): 187-193.

EFFECT OF VANADIUM POISONING AND VANADIUM PASSIVATION ON THE STRUCTURE AND PROPERTIES OF REHY ZEOLITE AND FCC CATALYST

Huai-Ping Wang*, Fang-Zhu Wang, and Wen-Ru Wu

State Key Laboratory of Heavy Oil Processing, University of Petroleum, Dongying 257061, CHINA

Keywords: REHY-zeolite, FCC-catalyst, passivator

INTRODUCTION

The effects of vanadium and nickel contaminants on the performance of cracking catalysts are well known [1,2]. These metals are deposited continuously on the catalyst during the cracking reaction and promote dehydrogenation reactions, which result in an increased formation of coke and light gases. Vanadium has an additional effect of reducing catalyst activity and selectivity by destroying zeolite crystallinity. Antimony passivation is widely practiced to control the effect of nickel poisoning [3], while vanadium poisoning is more difficult problem. Although much work has been done in the field, the exact mechanisms of the interaction of vanadium and zeolite and of the passivator for vanadium tolerance are still a matter of controversy [2,4-5]. However, application of a vanadium passivator in commercial FCC units also verified that a vanadium passivator can reduce the effect of the activity and the dehydrogenation by 30-50% and 65%, respectively [6].

Until recently, the vanadium passivation processes discussed extensively in the literature [7-9] involved addition onto the FCC catalyst of many different passivators, including rare earth metal oxides and alkali-earth metal oxides. These vanadium passivators can react with vanadium acid or V_2O_5, forming stable high melting compounds in the FCCU regenerator, so that vanadium poisoning is reduced and the crystal structure of zeolite is well protected.

In this paper, the mechanism of vanadium poisoning and vanadium passivation is proposed. The crystal structure of zeolite and its activity were well correlated with cracking activity.

EXPERIMENTAL

Catalyst Preparation and Evaluation

The RHZ-300 type cracking catalyst used in this work is a commercial heavy oil FCC catalyst composed of more than 30% REHY zeolite imbedded in 65-70% SiO_2-Al_2O_3-Kaolin matrix. The RHZ-300 catalyst and REHY (rare earth HY) zeolite were supplied by the Catalyst Factory of Qilu Petrochemical Company, Zibo, Shandong, China.

The vanadium poisoning of cracking catalyst procedure is used to impregnate RHZ-300 catalysts to the desired vanadium level with ammonium metavanadate solutions of different concentrations. The RHZ-300 catalysts contained 6000 ppm vanadium were then impregnated respectively with an acetate (such as lanthanum, magnesium, calcium, and so on) at various mole ratios of the passivator metal element to vanadium. After drying for 24 h at120• and calcination at 550°C for 4 h in air, the metal-loaded catalysts were aged at 760°C for 6h in 100% steam. The catalysts without vanadium passivators experienced the same procedure.

The catalyst's cracking activity was evaluated by a MAT test similar to one described by the RIPP-92-90 procedure [10] of The Research Institute of Petroleum Processing, China. The conditions of the MAT testing were 460°C for 70 s, catalyst-to-oil ratio = 3.2, WHSV (h-1) = 16,

*To whom correspondence should be addressed.

5.0 g catalyst, and the feedstock was a 1.56 g Dagang straight-run light diesel oil boiling range 230-350°C. The compositions of the products were analyzed using SQ-206 gas chromatography.

Catalyst Characterization

The relative crystallinity of the zeolite in the catalyst was obtained from the peak intensities of (533) plane of Y zeolite by XRD method with a Rigaku D/max IIIA X-ray diffractometer using Cu Kα radiation. The surface acid sites were characterized by NH_3-TPD-TG technique with a CAHN-200 thermal balance in the presence of a nitrogen atmosphere. The heating rate was 8°C /min. Analysis of the BET surface area and pore volume was measured by liquid nitrogen adsorption static state capacity method with an ASAP 2010 Multifunction Physisorption Instrument. Coke deposition on the catalyst was carried out in a micro fixed-bed reactor.

RESULTS AND DISCUSSION

The Effect of Vanadium Poisoning on the Cracking Activity and the Coke Formation of the RHZ-300.

The different effects of vanadium on the RHZ-300 cracking activity and coke formation are illustrated in Table 1. As shown in Table 1, microactivity monotonically decreased and the coke formation increased gradually with vanadium levels deposited on the catalyst. Little effect of MAT was observed up to 4000 ppm as vanadium, but above that amount, the activity decreased markedly with vanadium. Particularly, the coke formation on the catalyst was high when the deposition of vanadium reached 6000 ppm, a result consistent with the findings in the literature [11]. It is well known that the deposited vanadium reduces catalyst activity and selectivity and has catalytic activity towards dehydrogenation after aging at hydrothermal conditions, so that the dehydrogenation increases with vanadium levels, leading to an increase in the coke formation and a decrease in selectivity.

TABLE. 1. Microactivity and coke formation vs vanadium deposition on the catalyst.

V/×10³ppm	0	2	4	6	8	10
MAT/wt%	80.40	76.12	72.01	54.32	51.47	31.53
Coke yield/wt%	0.54	0.61	0.72	0.96	1.35	1.72

Vanadium Passivator Study

The effectiveness of one and two active constituent passivators prepared by loading on RHZ-300 individuality and mixture of rare earth oxides and alkali-earth oxides is shown in Table 2. As shown in Table 2, all active constituents are effective for vanadium passivation. However, vanadium passivation of performance of any one and two active constituent passivators was inferior to that of the pure lanthanum type. The vanadium passivator with a rare earth as the active constituent has an advantage over others in microactivity of RHZ-300, but the vanadium passivator with alkali-earth oxides as the active constituent greatly decreased the coke yields of RHZ-300. The phenomenon is primarly that the rare earth is weaker than alkali-earth oxide in neutralizing strong acidic sites of the catalyst, but greatly improves vanadium tolerance, whereas alkali-earth oxides easily neutralize excessively acidic sites, including weak acid sites and middle strong acid sites, owing to having strong basicity, leading to difference in activity and selectivity of RHZ-300.

TABLE 2 Vanadium passivation performance of the active constituents of passivators

Samples	Blank	La	Mg	Ca	La-Mg	La-Ca	La-Ce	La-Sr
MAT/wt%	54.32	72.88	67.34	64.46	69.87	67.56	71.74	67.76
Coke yield/wt%	0.96	0.75	0.53	0.56	0.65	0.67	0.73	0.69

The Effect of Vanadium Poisoning and Introduction of Passivator on the Structure and Microactivity of RHZ- 300

It is shown in Table 3 that after poisoning of the RHZ-300 catalyst by vanadium, the crystallinity of the REHY zeolite in the catalyst decreased from 10.5 % to 4.7%, a 55.2% reduction. Similarly, the BET surface area and pore volume of catalyst decreased respectively 55.3% and 7.8 %. This could indicate that the crystal structure of REHY zeolite in RHZ-300 was severely destroyed. Zeolite is often the cracking activity center of an FCC catalyst, and the activity drop could certainly be due to the destruction of zeolite structure. The reaction data from the MAT cracking testing (Table 3) verified that the microactivity of catalysts decreased from 80.4% to 54.32 %, while the coke formation increased from 0.80% to 0.96 %, as compared before and after poisoning with vanadium. These results agree with the conclusion made by Occelli et al [2]. The addition of passivator could prevent vanadium from poisoning the activity and selectivity of a FCC catalyst, so that the physicochemical and catalytic properties of RHZ-300 improved markedly, and the crystal structure of zeolite was recovered partially.

TABLE 3. Crystal Structure and Activity of Three Samples as Measured by Surface Area (BET), Pore Volume, XRD, Coke Formation, and Microactivity after Calcination at 550• and Hydrothermal Treatment at 760°C

Sample	RHZ-300	RHZ-300+V	RHZ-300+V+Passivator
MAT/wt%	80.4	54.32	75.60
Coke yield/wt%	0.80	0.96	0.65
BET S.A /$m^2.g^{-1}$	135.7	60.6	130.9
Pore volume/$cm^3.g^{-1}$	0.192	0.177	0.182
Crystallinity/%	9.7	4.7	7.2

Effect of Vanadium Poisoning and Introduction of Passivator on the Acidity of and Catalyst

Amounts of desorbed NH_3 were determined with the NH_3-TPD-TD method. The data of Table 4 show that total acidity of catalyst decreased from 2.21 to 1.08 after vanadium poisoning, indicating that over 50% of acid sites were destroyed. The distribution of acid intensity also indicated that acid sites destroyed were primarily weak acid sites and middle strong acid sites, over 65% of acid sites were destroyed whereas the middle strong acid sites have middle intensity adsorption, offer primary acid sites of catalytic activity. Cracking catalytic activity decreased greatly with the amounts of middle strong acid sites. In contrast, the amounts of strong acid sites increased from 0.37 to 0.45, so that the selectivity to coke formation could have an adverse effect (Table 4), since the coke is formed on the strong acid sites by polymerization of the unsaturated hydrocarbon molecules. The introduction of passivator (La_2O_3) can protect some of the acid sites leading to an increase in the number of acid sites of catalyst.

TABLE 4: Effect of Introduction of Vanadium and Passivator on Acidity of FCC Catalyst after Calcination at 550°C and Hydrothermal Treatment at 760°C

Sample	Acid sites (Desorbed NH_3 Amounts / $mmol.g^{-1}$ Cat.)			
	Weak acid sites	Middle strong acid sites	Strong acid sites	Total acid sites
RHZ-300	1.29	0.55	0.37	2.21
RHZ-300+V	0.45	0.18	0.45	1.08
RHZ-300+V+La_2O_3	0.94	0.55	0.38	1.87

Mechanism of Vanadium Poisoning and Passivation

In order to investigate interaction of zeolite and vanadium, steam-aging (at 760°C) experiments of REHY zeolite (with and without vanadium) were carried out in a flowing tube reactor. Fig. 1a shows the XRD pattern of REHY zeolite without vanadium; the crystal structure of zeolite is

completely retained without loss of crystallinity. Fig. 1c shows XRD pattern of the 2% vanadium-loading REHY zeolite. As evidenced by Fig. 1c, the zeolite completely loses crystallinity after vanadium poisoning, as the zeolite structure collapses with the formation of mullite ($Al_6Si_2O_{13}$), silica (tridymite) and rare earth vanadate ($CeVO_4$). The X-ray diffractograms for RHZ-300 catalysts with vanadium in the presence of steam at 760°C for 6 h are shown in Fig. 2a. It is very similar to the vanadium-loading REHY zeolite structure collapse with the formation of mullite. The above results and literature [2] suggest that the vanadium first deposits on the outside of the zeolite and catalyst particles, then migrates to pores, channels, or cages of the zeolite and catalyst and reaches acid sites during steaming at high temperature, where besides neutralized acid sites vanadium is trapped as cationic VO_2^+ species poisoning the catalyst according to the following reactions:

$$V_2O_5 + 2H^+\text{-}Y = 2VO_2^+\text{-}Y + H_2O \qquad [1]$$
$$VO_2^+\text{-}Y + 2H_2O = H^+\text{-}Y + H_3VO_4 \qquad [2]$$

Vanadic acid is a strong acid, P_K= 0.05 [20]. It behaves as a catalyst in the hydrolysis of the framework Al-O and Si-O tetrahedra and contributes to the accelerated destruction of the zeolites, causing zeolite de-alumination and lattice collapse with total loss of catalytic activity. The amorphous product recrystallizes then into mullite and the excess silica forms tridymite (Figs. 1c, 2a, 2b).

In REHY crystals it is believed that Ce^{4+} ions, present as an oxycerium complex, is preferentially loaded near the supercages, where it can more readily react with the stable oxyvanadyl cations (VO_2^+ or VO^{2+}) and form $CeVO_4$ (Fig. 4c).

The deleterious effects of vanadium deposits on zeolite-containing FCC can be greatly reduced by addition of certain materials (vanadium passivators) capable of minimizing V-FCC interactions by selectively (and irreversibly) sorbing migrating vanadium compounds such as H_3VO_4 (Figs. 1b, 2b). Since vanadic acid is not consumed as a catalyst in the hydrolysis reaction of framework. When a basic species exists in this system, it will compete with the zeolite for vanadic acid to form stable orthovanadates. The rare earth oxides such as La_2O_3 and alkali-earth metal such as MgO have basicity and react with vanadic acid to form orthovanadates, which are stable even at the highest temperatures reached in the regenerator unit.

Fig. 3 shows DTA thermograms of La_2O_3, V_2O_5, and the mixture of La_2O_3 and V_2O_5. There is a strong endothermic peak at 668°C in Fig. 3b, indicating the melting of V_2O_5. The strong exothermic peak at 670°C in Fig. 3c is probably an indication that a new compound is formed from the reaction of La_2O_3 and V_2O_5 as the melting point of V_2O_5 was reached. The XRD pattern (Fig. 4) verified the above observation that $LaVO_4$ indeed formed via the reaction, exhibiting the vanadium passivation by La_2O_3.

The DTA thermograms of MgO and V_2O_5 are shown Fig. 5, which were similar to Fig. 3. A strong exothermic reaction between MgO and V_2O_5 occurred at 670°C, and the reaction product characterized by XRD was MgV_2O_6 and $Mg_2V_2O_7$ (Fig. 6).

CONCLUSIONS

This study shows that when vanadium is deposited on a REHY zeolite and a RHZ-300 catalyst, the surface area, pore volume, crystallinity, acidity, and cracking activity of the vanadium-loading catalyst decrease with vanadium levels after aging at hydrothermal condiotion. In addition, vanadium forms a volatile vanadic acid during steaming at high temperature, which then catalyzes the hydrolysis of the framework Al-O and Si-O tetrahedra causing the collapse of the zeolite structure with the formation of mullite ($Al_6Si_2O_{13}$), silica (tridymite) and rare earth vanadate ($CeVO_4$). The activity and acidity of catalyst is completely lost at the same time. In contrast, the deleterious effects of vanadium deposits on zeolite-containing FCC catalyst can be greatly reduced by addition of certain vanadium passivators. The rare earth oxides and alkali-earth metal oxides are efficient passivators because they trap vanadium in form of vanadates, which are stable high melting compounds. Vanadium passivation reduces the

hydrolysis of zeolite framework, preserves the crystal structure of zeolites and acidity of FCC catalysts, and enhances the activity and selectivity of FCC catalyst. The optimum La/V mole ratio among the vanadium and La impregated catalysts (0.75) was obtained at the highest microactivity (72.88 wt%).

REFERENCES

1. Ritter, R. E., Rheaume, L., Welsh,W. A.,and Magee, J. S., Oil & Gas J.,103 (July 6,1981).
2. Occelli ,M. L., Catal. Rev. Sci. Eng., 33, 241 (1991).
3. McKay, D.L., Hydrocarbon Process, 97 (1987).
4. Pine, L. A., J .Catal.125,514(1990).
5. Trujilo, C. A., Uribe, U. N., Knops-Gerrits., et al., J. Catal.1, 186 (1997).
6. Barlow, R . C., et al., "NPRA Annual Meeting, 1986" AM-86-57.
7. Feron, B., Gallezot, P., and Bourgogne, M., J. Catal. 134, 469 (1992).
8. Chao, K. J., Lin, L. H., and Ling, Y. C., Appl. Catal. 121, 217 (1995).
9. Wormsbecher, R. F., Peters, A.W., and Maselli, J. M., J. Catal.100, 130 (1986).
10. Cuiding, Yang., et al., The Methods of Petroleum Processing, Science Press, Beijing, 1990.
11. Boock, L.T., Petti, T. F., and Rudesill, J. A., Preprints, ACS Div. Petrol. Chem., 40, 421, (1995).
12. Pope, M. T., in "Comprehensive Coordination Chemistry" (G. Wilkinson, Ed). Vol.3, p. 1026, Pergamon. Oxford.1987.

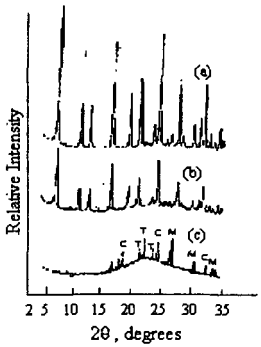

Fig. 1 X-ray diffractograms of REHY crystals steam-aged: (a) REHY, (b) REHY + 2%V + Passivator, (c) REHY + 2%V
M-Mullite ($Al_6Si_2O_{13}$), T-Sillica (tridymite)
C-Cerium vanadate ($CeVO_4$)

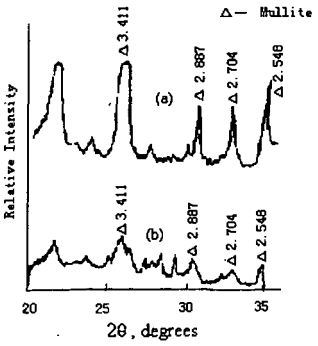

Fig. 2 X-ray diffractograms of catalysts with or without V-passivator: (a) no passivator, (b)passivator added

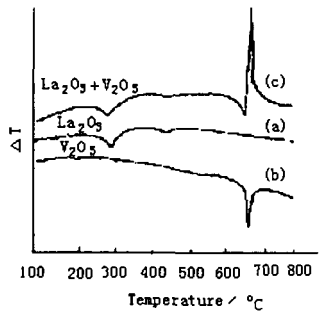

Fig. 3 DTA thermograms of La_2O_3, V_2O_5 and mixture of La_2O_3+V_2O_5 = 1 (mole ratio)

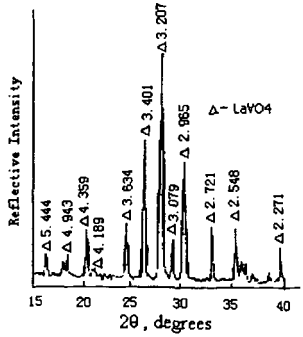

Fig. 4 X-ray diffractogram of the reaction product of La_2O_3 with V_2O_5

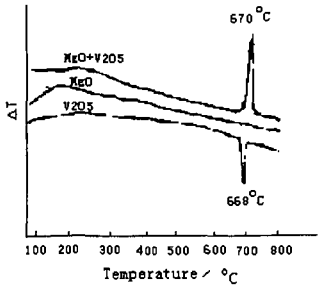

Fig. 5 DAT thermograms of MgO, V_2O_5 and mixture of $MgO/V_2O_5 = 1$ (mole ratio)

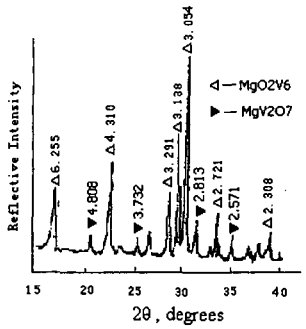

Fig. 6 X-ray diffractogram of the reaction product of MgO with V_2O_5

MOLECULAR DESIGN OF USY ZEOLITES USED FOR THE FCC PROCESS*

Xin-Mei Lui, Zi-Feng Yan**, Ling Qian, and Chun-Min Song

State Key Laboratory for Heavy Oil processing, University of Petroleum, Dongying 257062, CHINA

ABSTRACT USY zeolites, ultrastablized in hydrothermal treatment, were further modified by orthogonal design method with tartaric acid in an unbuffered system. The crystal structure, surface area and pore distribution, B acid sites and L acid sites, stability, and the activity for catalytic cracking of the modified samples were characterized by XRD, N_2 adsorption, FT-IR, DTA, and MAT. The research shows that the Si/Al ratio and the relative crystallinity of modified samples are both reasonably increased. Moreover, the pore system is developed further and the secondary mesopores are significantly greater than in the parent zeolites. The study has also shown that modified zeolites are preferable to deep cracking catalyst for producing lighter olefins and diesel oil with good yield and selectivity.

Keywords: USY; modification; tartaric acid; Si/Al ratio; pore distribution; activity; selectivity; lighter olefins

INTRODUCTION

Catalytic cracking process has been one of major techniques for lightening heavy oil. It not only plays an important role in petroleum refining, but also it is one focus that people pay close attention to. The success of the catalytic cracking is mostly attributed to the development or modification of the catalyst. With the cracking gasoline octane number boost, environmental concerns and deeper conversion of residual and heavy oils, especially the employment of reformulated gasoline, and the requirement for lower carbon olefins is dramatically increased. It is an effective way to produce much lighter olefins by further modification of zeolites existing in mordent FCC industry. Simultaneously, it is useful to the research of the design or modification of the catalyst structure.

Our efforts have been devoted to strengthening of the acidity and expanding of the mesopore of the USY zeolite by extraction of aluminum with tartaric acid whose negative ions has great complexing ability for Al^+. The negative ions and proton ions act in concert to Al-O band, which can achieve the de-alumination from the framework of the zeolites. The samples were prepared by orthogonal design (OD). The crystal structure parameter, physical adsorption property, stability, catalytic property of the modification zeolites was researched systematically by XRD, N_2 adsorption, FT-IR, DTA and MAT. The weight factors of effecting on the modification USY zeolites and optimum amount of each factor were explored.

EXPERIMENTAL

Materials and instruments

The parent USY zeolites were provided by Zhoucun Catalyst Company with the Si/AI ratio of 8.3, the unit cell constant of 24.528 Å and the relative crystallinity of 68.2%. Its crystal lattice was basically complete in the unbuffered acid system with the pH value above 2.0.
Type 79-1 magnetic heating agitator was purchased from Zhongda Instrument Plant in Jiangsu.

* This program is financially supported by Natural Science Foundation of Shandong Province.

** To whom correspondence should be addressed

Sample Preparation

A series of modified USY samples were synthesized by sol-gel method according to a L_4^5 orthogonal design table, in which the strong interactions among the parameters, such as addition volume of tartaric acid, solvent pH value, solvent volume and temperature were practically considered. The modified zeolite was washed by the distilled water to pH = 7, then filtered and dried for 14 hours at the temperature of 200°C.

Characterization of the Samples

The Si/Al ratio, unit cell constant, and relative crystallinity of the modified zeolite were determined by XRD with a Ricoh D/Max-IIIA X-Ray diffractometer using Cu Kα radiation. The pure NaY zeolite was used as calibration material. The Si /Al ratio was estimated from angles of 31~32 (2θ) XRD peaks.

The temperature of zeolite structure collapse was determined by DTA, with a CDR-1 DTA instrument of Shanghai Balance Instrument Plant.

The surface area and pore size distribution of modified samples were monitored by N_2 adsorption with a Macromectics ASAP 2010 unit.

Activity for catalytic cracking of Shenghua heavy oil (343°C-515°C) was carried out at 823 K near atmospheric pressure in a fixed-bed stainless steel reactor. The catalyst, which consists of 30% modified zeolites and 70% pretreated kaolin, was heated at 1073 K in a flow of water vapor for 4 h prior to introducing into reactor. The gaseous products were analyzed by HP-5890II gas chromatography equipped with a FID and a 50 m fused silicon capillary column. The liquid part was identified from simulated distribution on a HP-5880A with a FID and a 508mm fused UCW-982 column.

The number of acid sites was determined by FT-IR.

RESULTS AND DISCUSSION

The relation of the weight factors

The L_4^5 OD table is employed to find out the optimum synthesis conditions and investigate the interactions among factors. The SiO_2/Al_2O_3 ratio, mesopore (20 ~ 80 Å) volume and micro-activity are used to evaluate the performance of the modified USY zeolites. It is found that the order of the weight factors for above parameters employed is tartaric acid volume > pH value > solvent volume > temperature > reaction time.

The crystal parameters

The results of XRD show that the Si/Al ratio of the modified samples is obviously increased compared to the parent zeolites because the crystal unit cell content dramatically decreased, as observed in Table 1. This means that nearly only Al is extracted and therefore the skeletal Si/Al ratio is increased. The extracted Al dissolves in diluted de-alumination reagent solution and only partially remains in the zeolites. Owing to the stereo effect of the de-alumination acid, the frameworks Al is first depleted in the surface or subsurface and subsequently dissolves in solution. A similar transformation has been observed as a consequence of $(NH_4)_2SiF_6$ used for the treatment of a NaY zeolite [1]. Here, the higher relative crystallinity value of the de-alumination samples when compared to the parent zeolite may suggest that part of the framework be rebuilt. It can also be attributed to some changes in the physico-chemical properties (Si/Al ratio and extraction of the non-framework aluminum), which may influence the relative intensities of the X-ray diffraction peaks in the characteristic region of 2θ [2]. In addition, we also observed that when the relative crystallinity reaches the maximum, the content of crystal silicon of zeolite sample will amount to the maximum too, but the largest Si/Al ratio may not be obtained at this moment. This indicates that there is a portion of non-framework silicon existing in the zeolite. Furthermore, with the increase of silicon to aluminum ratio and decrease of crystal unit cell, the thermal stability of the modified zeolites is improved. This has been confirmed by the results of DTA. According to the OD results, it is postulated that the optimum modification conditions could be that the tartaric acid volume is 40 ml, pH value of solution is 1, the solvent volume is 40 ml, and the reaction time is 4 h.

Pore distribution

We always hope that the active component of FCC catalyst should possess structure with developed secondary mesopore. On the one hand, the larger reactant molecules may enter the pore channels of zeolite. On the other hand, it can decrease the molecular diffusion resistance to the zeolite cages. Thus the speed of the molecular diffusion is faster than the chemical reaction speed in the pores, which makes the activity sites of the pore be effectively used and the activity of the catalyst increased. This results in the catalyst efficiency improved. Fig.1 shows that the pore distribution of modified samples displays remarkable variation as a result of the tartaric acid treatments. The amount of secondary mesopores is distinctly increased. This refers not only to the mesopore volume, but also to the content of mesopore (20 ~ 80 Å). It reveals that the de-alumination is accompanied by the formation of some skeletal vacancies or defects. This vacancy or defect can be replenished by non-framework Si to complete the substitution of Al with Si. It can also be used to enlarge the pore mouth to form secondary mesopore. The enlarging of the pore mouth is attributed to the connection among the framework vacancies or defects by the interruption points created by the extraction of aluminum. All this leads to an increase of the amount of the secondary mesopores. Here the secondary mesopore formation is superior to silicon substitution because of the less enough silicon sources. It is worth mentioning that the amount of micropores is also increased, moreover, the micropore volume is enlarged. This may be achieved not only from the rebuilding of the framework, which leads to the larger mesopore changing into several micropores, but also from the enlarging of existing micropore (such as hexagonal column cages) that can not be tested by nitrogen adsorption. The optimum pore diameter of USY zeolite for processing heavy or residual oil should be in 20 ~ 80 Å, because the average van der Waal radius of the molecule residual and heavy oil, is 25 Å. Thus, the pore of 20 ~ 80 Å might be employed to evaluate the OD performance. The superior OD conditions are deduced as follows: the tartaric acid volume is 20 ml, pH value of solution is 3, the solvent volume is 40 ml, the temperature is 363 K and the reaction time is 6 h.

Acid property

The active sites of catalytic cracking reaction are acid components of the zeolites. Catalytic acidity of USY zeolites is attributed to acidic aluminum sites in both framework structure and non-framework debris [3]. Thus the extraction of the aluminum either from framework or non-framework of the zeolites should decrease the number of acid sites. The results of FT-IR really prove that the number of acid sites of the modified samples is decreased with the increase of Si/Al ratio. The Bronsted acid lies in the 1540 $cm^{-1}$and Lewis acid is in 1450 cm^{-1}, which is accordance with the literature [4,5]. The results are shown in Fig. 2.

Activity and selectivity

The MAT data reveal considerable changes as a result of the tartaric acid treatments. The results are shown in Fig. 3and Fig. 4. From the above results, it can be seen that the modified USY samples possess the more reasonable pore system structure, the greater SiO_2/Al_2O_3 ratio, and better distributed aluminum, which leads to the selectivity of all kinds of object product improved. The acidity of USY zeolites governs their activity. So with the de-aluminating, the active sites are decreased. But with the increase of the secondary mesopores and the enlarging of average total pore openings, the activity sites are effectively used. Though the acid sites are decreased, the catalyst total activity is not dropped clearly; conversely, some catalyst's activity is improved. This change is exhibited by the conversion change as the results of Fig.3. Moreover, the extraction of aluminum results in the increase of acid strength, which restrains the inter-molecular hydrogen migration of hydrocarbon intermediates. So the selectivity to the $C^{=}_3$ ~ $C^{=}_6$ hydrocarbons in the gas is raised, however, due to the difference of the gas selectivity of each catalyst, the yield of the $C^{=}_3$ ~ $C^{=}_6$ hydrocarbons is less even if selectivity of some catalysts is greater. The deep conversion is a tendency for FCC process. It is controlled by accumulation of coke on catalyst surface not by activity of catalyst. Thus, the selectivity of the coke is the principal focus to which attention is paid. In order to prolong the catalyst life span and reduce the load of its regeneration, we always hope that the coke yield is as low as possible in the case of satisfying our need for the object products. Fortunately, our goal is achieved. The decrease of the coke has two reasons. One is the increase of the acid strength; this leads to the reduction of the speed of condensation reaction. The other is the decrease of the external

surface area; this cuts down the chances of the inter-molecular hydrogen migration reaction that can produce coke. According to the results, it is postulated that the optimum modification conditions are the same as the pore distribution conditions. Using this modified zeolites, the products distribution are as follows: the light oil yield is 69.4%, the coke yield is decreased from 3.73% to 3%, the selectivity and the yield of $C^{=}_{3}-C^{=}_{6}$ are respectively 51.7% and 15.53%.

CONCLUSIONS

The results indicate that it is a new effective method to modify USY zeolites with tartaric acid in the unbuffed system. In this way, the thermally more stable samples with higher SiO_2/Al_2O_3 ratio, higher relative crystallinity, more well developed secondary mesopore system can be prepared. These samples may be benefit to heavy oil and residual oil deeper cracking. Furthermore, lighter olefins with good yield and selectivity may be obtained in the FCC procedure.

References

[1] P. Xie, Y. Zh. Zhang, L.B. Zheng, CUI HUA XUE BAO, 1991, p.

[2] R. Le Van Mao, S. T. Le, D. Ohayon, F. Caillibot, L. Gelebart, and G. Denes, Zeolites, 1997, p.270.

[3] Xiaolin Yang and Ralph E. Truitt, Zeolites, 1996, p.249.

[4] R. Beaunmont and D. Barthomeuf, J. Catal., 1972, p.218.

[5] G. T. Kerr, R. J. Mikovsky, U.S. Patent, 3,493,519 (1970).

Table 1. The crystal structure parameters of zeolites

Experiment order	Si/Al ratio	relative crystallinity C_{RX}%	crystal unit cell param. a_o/Å	content of crystal silicon S
1	10.2	64	24.463	157.6
2	10.1	65	24.466	159.7
3	10.4	66	24.460	162.7
4	10.6	67	24.455	165.8
5	11.6	68	24.435	170.4
6	11.6	67	24.435	167.9
7	12.6	68	24.419	172.1
8	10.4	69	24.461	170.1
9	12.9	68	24.415	175.1
10	12.8	66	24.416	167.4
11	10.8	77	24.451	191.1
12	11.0	74	24.448	184.0
13	11.9	75	24.431	188.4
14	12.2	77	24.427	194.0
15	11.9	72	24.431	180.9
16	12.2	77	24.426	194.1
Parent sample	8.3	68	24.528	161.0

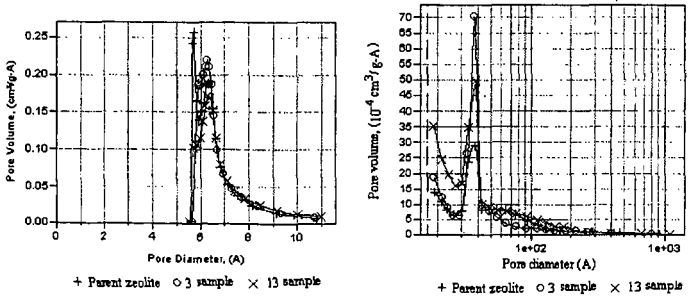

Fig.1 Profile of the pore size distribution of modification samples

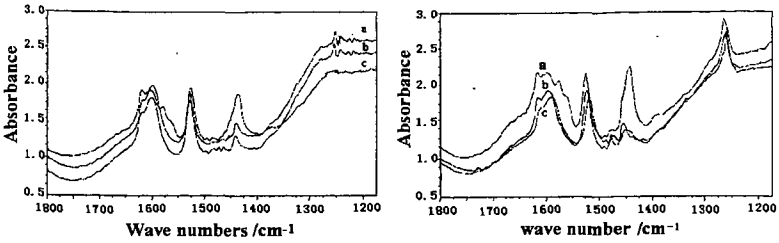

Fig.2. Profile of the acid site of modification samples. a---423K; b----523K; c-----623K

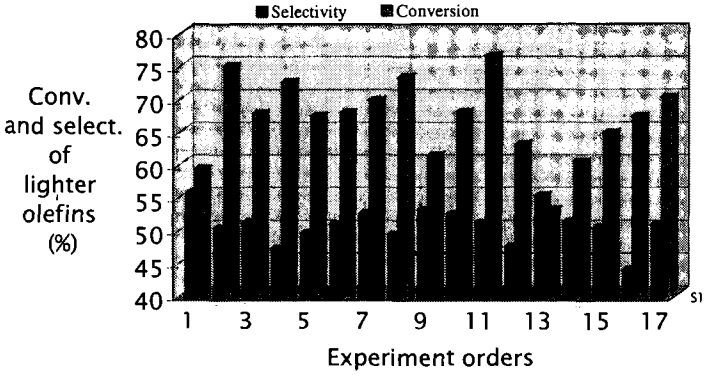

Fig.3 Profile of the conversion and selectivity of $C^{=}_{3}$-$C^{=}_{6}$

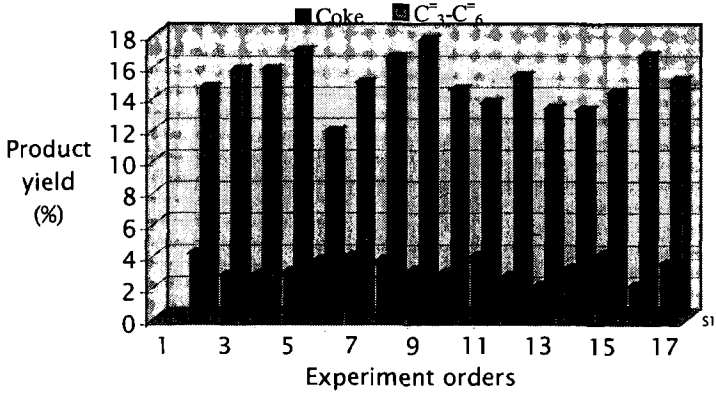

Fig.4 Profile of the product yield

EXTRACTING NUCLEAR ENERGY FROM HEAVY WATER WITH THE AID OF ELECTROCHEMISTRY

Andrew C. Angus,
Absolute Foundation,
2117 Wendover Lane, San Jose, California 95121, U.S.A.,
E-mail: andrewangus@yahoo.com.

KEYWORDS: heavy water, electrochemistry, low-energy fusion

INTRODUCTION

Heavy water, chemically known as **deuterium oxide**, is usually used as a moderator in nuclear reactors. However, two chemists, Stanley Pons and Martin Fleischmann, reported excess heat four times the energy output by electrolysing heavy water with the use of Palladium and Platinum electrodes and Lithium Deuteroxide as electrolytes. They believed that nuclear fusion occurred in their experiments. (Pons and Fleischmann, Ref.#3)

Did the two chemists made a mistake in their experiments? Or did Ernest Rutherford made a mistake in his theory of thermo-nuclear fusion reaction? Should experiments fit into a conventional theory? Or should theory fit experimental results?

What are the principles underlying nuclear fusion at low temperature?

In this paper, the author explains the theoretical foundations of nuclear fusion at low temperature with the aid of electricity and the new models of nuclear fusion.

METHOD

Electrolysis

The electrolysis of heavy water will yield two deuterium ions (D^+1) and oxygen ions (O^-2). Electrolysis is an endothermic reaction. About 118 kilojoules of energy must be supplied to form one gram of hydrogen. (Masterton p.97)

$$\text{Electricity} + \quad D2O \rightarrow (2D+) + O\text{-}2 \qquad \text{eq.1}$$

RESULTS

Electrochemical Reactions

The following are electrochemical reactions that occur in the Platinum anode and Palladium cathode in the Pons-Fleischmann experiment using the electrolyte Lithium Deuteroxide:

1. Deuterium Oxide (D2O)

$$\text{Anode} : O^{-2} \rightarrow O + 2e^- \qquad \text{eq.2}$$
$$\text{Cathode:} \ 2(D^{+1}) + 2(e^-) \rightarrow D^*2 \qquad \text{eq.3}$$

2. Lithium Deuteroxide (LiOD)

$$\text{Anode} : (OD^-) \rightarrow O + (D) + 1e^- \qquad \text{eq.4}$$
$$\text{Cathode:} \ (Li^{+1}) + e^- \rightarrow Li \qquad \text{eq.5}$$

3. Lithium Deuteroxide (LiOD) and Deuterium Oxide (D2O)

$$\text{Anode:} \ O\text{-}2 + (OD^-) \rightarrow 2O + D + 3e^- \qquad \text{eq.6}$$
$$\text{Cathode:} \ 2(D^{+1}) + (Li^{+1}) + 3(e^-) \rightarrow D^*2 + Li \qquad \text{eq.7}$$

Note: D*2 refers to a diatomic deuterium molecule.

Pons and Fleischmann reported excess heat energy four times the energy output. (Pons and Fleischmann, Ref#3) How is nuclear fusion possible in the Palladium cathode at low temperature/low energy?

DISCUSSION

A. What is the most important factor involved in Low-Energy Fusion?

In **muon-catalyzed nuclear fusion,** the muon (which is more massive than the electron) replaces the electron and induces the fusion of two nuclei. (Steven Jones, Ref. #2). In **electron-catalyzed nuclear fusion,** the electron must have an effective mass which will induce the fusion of two nuclei. (Barbara Levi, Reference #4)

K Capture is an important nuclear process which involves the increase of electron mass. Hence, K Capture is an essential process in electron-catalyzed nuclear fusion. K Capture, therefore, is the most important factor involved in Low-Energy Fusion.

B. What is K Capture?

K Capture *is the nuclear process whereby the nucleus absorbs its electron in the K Shell,* the nearest energy shell. (Weber p. 868)

C. When does K Capture occur?

Conventional theory states that heat induces K Capture. The author gives an alternative theory whereby electricity induces K Capture.

The author theorizes that K Capture occurs when electricity increases the mass of electron in the K shell at a critical level that the binding energy (hf) needed in maintaining the massive electron in the K shell is not sufficient anymore. Consequently, the repulsive force barrier of the nucleus collapses and the electron is absorbed by the nuclear proton forming a new neutron or, **neo-neutron** (n-1) to differentiate it from the old neutron in the nucleus. Meanwhile, if deuterium undergoes K Capture, the by-product is called **di-neutron** (n-2) which is simply a fused neutron pair.

D. How does K Capture occur?

Let us use Hydrogen as our example. The energy that prevents the absorption of electron by the nucleus is the binding energy of the photon (hf) possessed by the atom. If the Hydrogen atom is treated with electricity, the electron mass will increase in direct proportion to the current amperage and time. The resulting electron that increased in mass is called a **superelectron** or **heavy electron.** As the electron's mass increases, the atom's binding energy (hf) needed in maintaining the heavy electron at the K shell is not sufficient anymore since the kinetic energy of the heavy electron has increased due to an increase of electron mass. The kinetic energy (1/2 mv^2) of the heavy electron has become greater than the atom's binding energy (hf). At a certain critical electronic energy (qV) and critical mass (m) of the electron, the atom's repulsive force will collapse and the heavy electron will be absorbed by the nuclear proton to form a new neutron or **neo-neutron** (n-1). When the nucleus absorbs the heavy electron, the binding energy (hf) will be emitted by the nucleus.

E. An example of K Capture Equation

The reaction-equation of the K Capture of Deuterium is as follows:

$$3MeV + D \longrightarrow n\text{-}2 \qquad \text{eq. 9}$$

Legend: D stands for deuterium, n-2 stands for dineutron particle.

F. What are the Laws of K Capture?

The author formulates mathematical equations called the Laws of K Capture to explain the mechanism of K Capture as induced by electricity.

i). First Law of K Capture: The new electron mass (m) is equal to amperage (I) multiplied by time (t), then, multiplied by J.J. Thomson's ratio (k) of electronic mass to electronic charge (q).

$$I \times t \times k = m. \qquad \text{eq. 10}$$

$$q \times k = m \qquad \text{eq. 11}$$

The first Law of K Capture was derived as follows:

$m \alpha I$ eq. 12
$m \alpha t$ eq. 13
$m \alpha It$ eq. 14
$m / It = constant$ eq. 15
$It = q$ eq. 16
$m / q = constant$ eq. 17
$m / q = k$ eq. 18
$q \times k = m$ (eq. 11)

The first Law of K Capture is called the **Law of Electron Mass Accretion**.

ii). Second Law of K Capture: The net kinetic energy of the absorbed electron is equal to the electronic energy (qV) minus the energy (W) needed to overcome the repulsive energy barrier of the nucleus.

Net K.E. (absorbed electron) = qV– W eq. 19

The Second Law of K Capture is called the **Law of Electronuclear Effect.**

iii). Third Law of K Capture: The net kinetic energy of the absorbed electron is transferred to the new neutron formed. Thus, the net kinetic energy of the new neutron is equal to the net energy of the absorbed electron.

Net K.E.(neo neutron) = Net K.E.(absorbed electron) eq. 20

iv). Fourth Law of K Capture: The net kinetic energy of the neo-neutron formed is equal to the electronic energy (qV) minus the energy (W) needed to overcome the repulsion barrier. From eqs. 12 and 13, we derive:

Net K.E. (neo neutron) = q V – W. eq. 21

v). Fifth Law of K Capture

Now, the following condition show when K Capture will occur or will not occur.

i). If qV = W, then K Capture will not occur. eq. 22
ii), If qV < W, then K Capture will not occur. eq. 23
iii). If qV >W, then K Capture will occur. eq. 24

The author introduced the Laws of K Capture in a paper presented in an international conference in Sta. Fe, New Mexico, U.S.A. (See Reference #1.)

G. What are electro-nuclear fusion models?

K Capture can be used to explain and unify the diverse unconventional results obtained in deuterium-related experiments by Steven Jones, Stanley Pons, Martin Fleischmann, Japanese scientists Yoshiaki Arata and Yue-Chang Zhang, etc.

Let us now introduce the new models of nuclear fusion. These are **K Capture-based nuclear reactions** called **electro-nuclear reactions** to differentiate it from Rutherford's thermo-nuclear reaction models of nuclear fusion:

a.) 3 MeV (electricity) + D*2 → n-2 + D → H-4 → T + n + 6.2 MeV eq. 25
b.) 3 MeV (electricity) + D*3 → n-2 + D2 → He-6 → 2T + 12.4 M eV eq. 26
c.) 3 MeV (electricity) + D*3 → n-2 + D2 → He-6 → He-4 + n-2 + 25 MeV eq. 27
d.) 3 MeV (electricity) + D*3 → n-2 + D2 → He-6 → He-3 + 3n + 4.15 MeV eq. 28

Note the following: **Eq. 9** shows that neutrons are formed but no excess nuclear energy is produced, thereby, explaining the negative energy result in the experiments of **Steven Jones.** (See Ref.#2) Eqs.18 shows that Tritium and neutrons are formed and nuclear energy is produced. **Eq. 26** shows that the energy output is four times the energy input which is exactly reported by **Stanley Pons and Martin Fleischmann** in March 1989. (See Ref. #3.) **Eqs. 27 & 28** show that Helium-4 and Helium-3 and excess energy are produced which explain the experiments of **Yoshiaki Arata and Yue-Chang Zhang.** (See Ref. #5)

H. What about the conventional thermo-nuclear fusion models?

The conventional thermo-nuclear reaction models of nuclear fusion of Ernest Rutherford cannot unify and explain the diverse experimental results of Steven Jones, Stanley Pons, Martin Fleischmann, Yoshiaki Arata and Yue-Chang Zhang.

Perhaps, we have to say good-bye to the following thermo-nuclear fusion reactions:

$D + D \rightarrow T + p + 4.03\ MeV$	eq. 29
$D + D \rightarrow He\text{-}3 + n + 3.27\ MeV$	eq. 30
$D + T \rightarrow He\text{-}4 + n + 17.59\ MeV$	eq. 31

I. Why is Plasmic State - Hot Fusion unsustainable?

Plasmic State - Hot Fusion Theory is feasible but not sustainable in accordance to the following argument:

a. Let us review the **Ideal Gas Law** which is well-known to chemists and physicists alike (equation 32) :

$$PV = nRT \qquad \text{eq. 32}$$

b. Let us derive "concentration density" from the Ideal Gas Law. How?

Let us define **concentration density** as the number of moles of an element per unit volume. We use the symbols C or n/V for concentration density.

$n / V = P / R T$	eq. 33
$C = n / V$	eq. 34
$C = P / RT$	eq. 35

R is the Rydberg Constant,
P is Pressure,
T is temperature,
n is the number of moles,
V is the Volume.

c. Equation 34 and 35 are called the **Laws of Concentration Density** which is one of the underlying principles of the Low-Temperature Nuclear Fusion Theory or Low-Energy Nuclear Fusion Theory.

d. High Concentration density is more achievable for hydrogen in a gaseous state in a solid state medium rather than hydrogen in a plasmic state confined in a magnetic bottle.

e. Plasmic state- Hot Fusion Theory is a **physical violation** of Equations 34 and 35. Plasmic state- Hot Fusion Theory can never achieve a sustainable nuclear fusion because the high temperature of a plasmic state induces a very low concentration density. Consequently, the probability of nuclear fusion is very low.

Consequently, the physics world must accept the Low-Temperature Nuclear Fusion Theory or Low-Energy Nuclear Fusion Theory.

CONCLUSION

The controversial claims of chemists Stanley Pons and Martin Fleischmann that they achieved nuclear fusion at low temperature in the historic year 1989 is clearly justified on the basis of new models of nuclear fusion called electro-nuclear reactions. Hence, physicists and chemists must welcome the theory of low energy - nuclear fusion and the new electro-nuclear reaction models of nuclear fusion.

We have to say good-bye to Rutherford's thermo-nuclear reaction models of nuclear fusion since the energy input, energy output, reactants and by-products observed in deuterium-related experiments do not commensurate if we use Rutherford's thermo-nuclear reaction models of nuclear fusion.

Indeed, heavy water is a good source of nuclear energy with the help of electrochemistry. Eventually, mankind is assured of a cheap, limitless and clean source of energy.

REFERENCE

1. Angus, Andrew (1999). "Mathematical Model of K Capture and Its Implications", paper presented as poster in the *10th International Symposium on Capture Gamma Ray and Spectroscopy* in Sta. Fe, New Mexico, U.S.A. last August 30-September 3, 1999.

2. Jones, S., Palmer, E.P. et. al. (1989). "Observation of Cold Nuclear Fusion in Condensed Matter. In: *Nature*, Vol **338**, April 27, 1989, pp. 737-740.

3. Fleischmann, M. and S. Pons. (1989). "Electrochemically Induced Nuclear Fusion of Deuterium". In: *J. Electroanalytical Chemistry*. **261.**

4. Levi, Barbara (1989). "Doubts Grow as Many Attempts at Cold Fusion Fail". In: *Physics Today*, June 19, 1989. p.19.

5. Arata, Y. and Y-C Zhang (1997). "Helium (He-4, He-3) Within Deuterated Pd-Black". In: *Proc Japan Acad.* Ser. B, 1997, 73.

6. Masterton, W. , Slowinski, Emil J. and Stanitski, C. (1985). *Chemical Principles,* 6th Edition. USA: Saunders College Publishing.

7. Weber, R., Manning, K., White, M. and George Weygand (1977). *College Physics*, 5th ed., New York: McGrawHill Book Co.,. P. 868.

CHEMICAL BONDING OF NEW ALLOTROPES OF HYDROGEN AND ITS IMPLICATIONS TO FUEL SCIENCE

Andrew C. Angus
Absolute Foundation
2117 Wendover Lane, San Jose, CA 95121, U.S.A.
angusandrew@yahoo.com

KEY WORDS: chemical bond, polyatomic allotropes of hydrogen, nuclear fusion

INTRODUCTION

The author predicts that polyatomic allotropes of hydrogen such as triatomic deuterium (D*3) and quadratomic deuterium (D*4) are formed inside the core of the sun.

The theoretical existence of triatomic deuterium molecules and other polyatomic allotropes of hydrogen in general is necessary in order to account nuclear fusion in the sun.

The theoretical existence of triatomic deuterium molecules and polyatomic allotropes of hydrogen if confirmed experimentally is important in fuel science since polyatomic allotropes of hydrogen increase the probability of nuclear fusion by virtue of their close distance to one another.

This paper explains the chemical bonding of *triatomic* and *quadratomic deuterium atoms* which can be applied to polyatomic hydrogen atoms in general.

MODELS OF CHEMICAL BONDS

1. Lewis Model of Chemical Bond

G. N. Lewis, an American physical chemist was the first to suggest that a **chemical bond** is composed of an "**electron pair**". (Masterton, p. 267)

The **Lewis model of chemical bond** in molecules or between atoms shows an electronic structure of a molecule or ion in which electrons are shown by dots or dashes (electron pairs). The Lewis model of chemical bonds does not show the actual physical models of the atoms. For example, the Lewis model of a diatomic hydrogen is *illustrated* as: *H : H or H-H.*

The Lewis model of chemical bond does not explain the possible existence of triatomic molecule of hydrogen or polyatomic allotropes of hydrogen in general.

2. Angus Model of Chemical Bond

The author proposes a chemical bond called "**single electron sharing**" between two atoms to explain the theoretical existence of a triatomic deuterium molecule, quadratomic deuterium molecule and higher polyatomic hydrogen molecules. This bond that is based on a "single electron sharing" is called "**mono-electron bond**" or "**alpha bond**". Hydrogen bonds between water molecule is a good example of an alpha bond or mono-electron bond.

Chemists failed to realize that the hydrogen bonding in water molecules and protein molecules could probably involve a "single electron sharing" bond.

The author coins the term "***di-electron bond***" *as a synonymous term to Lewis' chemical* bond of "**pair electron sharing**". The sigma bond is a good example of a "di-electron bond".

The "**quadri-electron bond**" is a "four-electron sharing" bond such as the chemical bond in an Oxygen diatomic molecule. The "quadri-electron bond" is synonymous to the "double bond".

The "**hexa-electron bond**" is a "six-electron sharing" bond such as the chemical bond in a Nitrogen diatomic molecule. The "hexa-electron bond" is synonymous to the "triple bond".

ILLUSTRATIONS

The author gives the illustrations of the allotropes of Hydrogen namely, **monatomic** hydrogen, **diatomic** hydrogen, **triatomic** hydrogen and **quadratomic** hydrogen:

1. Monatomic Hydrogen (H)

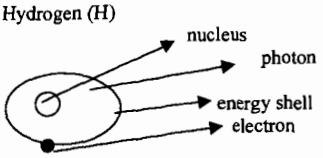

Monatomic Protium

Monatomic Deuterium

2. Diatomic Hydrogen (H*2)

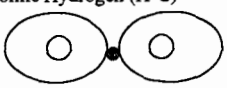

i).. **alpha bond**: single electron sharing

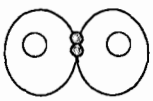

ii). **sigma bond**: pair electron sharing

3. Triatomic Hydrogen (H*3)

i). Chain structure of a triatomic protium molecule (H*3) and triatomic deuterium molecule (D*3).

2 alpha bonds in H*3 ion

2 alpha bonds in D*3 ion

ii). Ring structure of a triatomic protium molecule (H*3) and triatomic deuterium molecule (D*3).

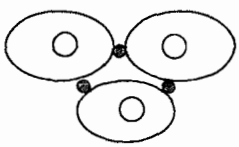

3 alpha bonds in H*3 molecule

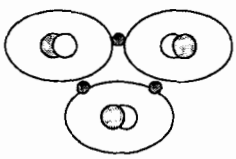

3 alpha bonds in D*3 molecule

4. Quadratomic Hydrogen (H*4)

i). Chain structure of a quadratomic protium molecule (H*4) and quadratomic deuterium molecule (D*4)

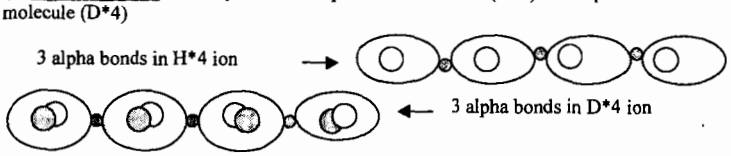

ii). Ring structure of a quadratomic protium molecule (H*4) and quadratomic deuterium molecule (D*4)

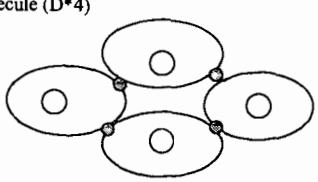

4 alpha bonds in H*4 molecule

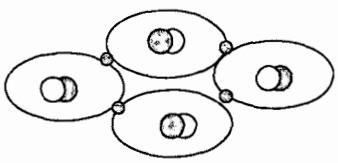

4 alpha bonds in D*4 molecule

DISCUSSION

A. Angus Model of an Atom

1. **Description.** The **Angus Model of the Atom** depicts atoms that looks like a "biological cell" with a central nucleus. The nucleus is surrounded by a quantum of energy or photon. The electron is at the surface of the photon. The **atom's energy realm** refers to the total area or volume occupied by the photon in an atom. The periphery of the photon is called the **atom's energy shell.** (See Illustration #1)

2. **Energy Barrier.** The electron cannot penetrate the nucleus because of the **photon energy barrier (hf).** The photon energy barrier (hf) is equal to the force (F) between the proton and the electron multiplied by the radius (r) distance between the nucleus and the electron.

$$F \times r = hf \qquad \text{eq.1}$$

3. **Photon Force.** The new model of the atom proposes that the force (F) between proton and electron is exerted through the medium of a photon energy (hf) that binds the electron and the nucleus at a certain distance (r). The force exerted by the proton on the electron through an photon energy medium is called a **photon force.**

$$hf / r = F \qquad \text{eq.2}$$

B. Angus Model of Chemical Bond

The Lewis Model of chemical bond of a **"pair electron sharing"** cannot account the new allotropes of Hydrogen namely the triatomic deuterium molecule (D*3) and the quadratomic deuterium molecule (D*4). The author's theory of chemical bond of **"single electron sharing"** called "alpha bond or mono-electron bond" can account the existence of new polyatomic allotropes of Hydrogen (such as D*3, D*4, D*5, etc.).

The concept of a "single electron sharing" of a diatomic hydrogen molecule was discussed thcoretically in physics textbook . (Kenneth Krane, p. 360-364.) But the author did not use it to explain the possible existence of polyatomic allotropes of hydrogen molecules/ions. Furthermore, the author claimed that the attractive force of the electron **is greater** than the repulsive force exerted by the protons on the electron. (Krane p.360)

I believe: If the electron's attractive force is greater than the repulsive force of the two protons (as claimed by Krane p.360), then the two protons will fuse towards the electron. Therefore, physicist's analysis of a "single electron sharing" between two atoms would make a mono-electron bond an unstable bond.

Is a mono-electron bond (or alpha bond) stable or unstable? I offer an alternative analysis of a "single electron sharing bond". The two protons are both attracted to the single electron. The attractive force of this single electron shared by two protons **is equal** to the two protons' repulsive force exerted on the electron. The electron maintains its distance equally to the two protons. The electron stays in the middle of the two protons. The electron is not absorbed by the two protons. Thus, a mono-electron bond is stable.

attractive force of electron on proton = $(1/4\pi\varepsilon)[e^2/(R)^2]$ eq. 3
attractive force of electron on 2 protons = $2(1/4\pi\varepsilon)[e^2/(R)^2]$ eq.4
repulsive force of proton on electron = $(1/4\pi\varepsilon)[e^2/(R)^2]$ eq.5
repulsive force of 2 protons on electron = $2(1/4\pi\varepsilon)[e^2/(R)^2]$ eq.6
attractive force of e- on two protons = repulsive force of two protons on e- eq.7
$2(1/4\pi\varepsilon)[e^2/(R)^2] = 2(1/4\pi\varepsilon)[e^2/(R)^2]$ eq.8

In Illustration #2, it can be gleaned that a diatomic hydrogen can either have an alpha bond (mono-electron bond) or a sigma bond (di-electron bond).

In the Illustration #3 (triatomic hydrogen) and #4 (quadratomic hydrogen), it can be gleaned that polyatomic allotropes of hydrogen in general can either have a chain structure or a ring structure.

In Illustration #3, triatomic deuterium has two alpha bonds since the K shell of deuterium can carry a maximum of two electrons. Instead of deuterium sharing the two electrons to one atom, deuterium is sharing one electron to each of the two atoms.

The nature of hydrogen bonding is a mystery to chemists. The author theorizes that hydrogen bonding occurs in water molecules when oxygen atom "share a single electron" to a neighboring hydrogen atom bonded to another oxygen atom.

C. Source of Polyatomic Hydrogen

I predict that triatomic deuterium (D*3) and quadratomic deuterium (D*4) and other polyatomic deuterium molecules exists in the sun. I believe that triatomic, quadratomic allotropes of hydrogen or polyatomic hydrogen atoms in general are the main fuel of the sun.

The sun has a high density 1.5 x 10^5 kg/m^3 about 13 times the density of lead, a high central pressure (approximately 2 x 10^11 atmosphere) and a central temperature of 1.5 x 10^7 Kelvin. (Halliday p. 1317)

The high pressure due to the gravitational pressure or the electromagnetic pressure in the sun could be the major factor in creating polyatomic hydrogen atoms such as triatomic deuterium (D*3), quadratomic deuterium (D*4), pentatomic deuterium (D*5), etc.

$$D + D + D + D + \text{pressure} + \text{electricity} \rightarrow D^*4 \qquad \text{eq. 9}$$

If nuclear fusion reactions occur in the sun, then hydrogen atoms must be close to each other as in a "chain of polyatomic hydrogen atoms" or a "ring of polyatomic hydrogen atoms". Nuclear fusion reactions would be difficult to occur if hydrogen atoms exist as monatomic atoms. Thus, to facilitate nuclear fusion, polyatomic hydrogen must exist in the sun since polyatomic allotropes of hydrogen consists of hydrogen atoms that are very close to each other.

The high density of the sun is probably due to helium atoms and polyatomic allotropes of hydrogen. Monatomic hydrogen atoms tend to be far apart when heated to extreme high temperatures. An abundance of monoatomic hydrogen atoms will create a low-density sun. An abundance of polyatomic allotropes of hydrogen will help in creating high-density sun.

D. Energy Mechanism of the Sun

Hans Bethe made a theory explaining the energy mechanism of the sun based on thermonuclear model of nuclear fusion whereby heat initiated nuclear fusion.

However, I believe Bethe's Theory cannot be totally correct for the following arguments: 1). Extreme heat will encourage the formation of monatomic hydrogen ions rather than triatomic and polyatomic allotropes of hydrogen atoms. 2). Monatomic hydrogen ions are so far apart that the probability of nuclear fusion will be greatly decreased. 3). Pure monatomic hydrogen atoms will create a low-density sun. 4). Nuclear reactions can occur in proto-stars or actual stars even at low energy or low temperature (as will be explained in the next paragraph).

An alternative energy mechanism of the sun (without resorting to high temperature) involves high pressure to create polyatomic allotropes of hydrogen and electricity applied on these polyatomic allotropes of hydrogen as follows:

Phase 1

$H + \text{pressure} + \text{electricity} \rightarrow n\text{-}1$ (K Capture of Hydrogen) eq.10

$H + H + \text{pressure} + \text{electricity} \rightarrow H^*2$ eq.11

$H^*2 + \text{pressure} + \text{electricity} \rightarrow n\text{-}1 + H \rightarrow D + 2.22\ \text{MeV}$ eq.12

Phase 2

$D + \text{pressure} + \text{electricity} \rightarrow n\text{-}2$ (K Capture of Deuterium) eq.13

$D + D + D + \text{pressure} + \text{electricity} \rightarrow D^*3$ eq.14

$D^*2 + \text{pressure} + \text{electricity} \rightarrow n\text{-}2 + D \rightarrow \mathbf{H\text{-}4} \rightarrow T + n + 6.2\ \text{MeV}$ eq.15

$D^*3 + \text{pressure} + \text{electricity} \rightarrow n\text{-}2 + D^*2 \rightarrow \text{He-}6 \rightarrow 2T + 12.4\ \text{MeV}$ eq.16

$D^*3 + \text{pressure} + \text{electricity} \rightarrow n\text{-}2 + D^*2 \rightarrow \text{He-}6 \rightarrow \text{He-}3 + 3n + 4.15\ \text{MeV}$ eq.17

$D^*3 + \text{pressure} + \text{electricity} \rightarrow n\text{-}2 + D^*2 \rightarrow \text{He-}6 \rightarrow \text{He-}4 + n\text{-}2 + 25\ \text{MeV}$ eq.18

(Note: **Protium** is defined as a proton with an orbiting electron. **Hydrogen** is defined as an element with a single proton. Protium (H), Deuterium (D), Tritium (T), Quadrium (Q) are the four isotopes of Hydrogen. **Quadrium (H-4 or Q)** occurs in the reaction in equation 15.)

K Capture is a nuclear process that involves the absorption of orbital electron in the K Shell. K Capture is a key factor in overcoming repulsive energy barrier of atoms at low temperature with the help of electricity. The process of K Capture with the help of electricity

converts Protium (H) into neutron (n-1) as shown in eq. 10. The process also converts Deuterium atom (D) into a di-neutron (n-2) as shown in eq. 13. (Angus 1999)

K Capture as induced by electricity is represented by the mathematical equation 19 called **Law of Electro-nuclear Effect** (Angus 1999):

$$\text{Net K.E. of electron} = qV - W \qquad \text{eq.19}$$

Meanwhile, the high pressure (Pb) in the sun will force the atoms to get closer to each other. Then, electrcity (qV) can increase the effective mass of orbital electron to produce neutrons or di-neutrons that will induce nuclear fusion of deuterium atoms. The repulsive energy barrier of the atoms can be overcome by the following equation whereby the orbital electron is subjected to the pressure (Pb) and the electricity (qV) in the sun:

$$\text{Net K.E. of electron} = (Pb + qV) - W \qquad \text{eq.20}$$

P is the pressure, b is the volume of the electron, q is the electronic charge, V is the voltage and W is the energy needed to overcome the repulsive energy of the atom.

Equation 20 is called the **Law of Piezo-electro-nuclear Effect** which explains K Capture as induced by pressure and electricity. This Law explains K Capture as a key factor in the energy mechanism of the sun or proto-suns at low energy or low temperature.

We can simulate the energy mechanism of the sun here on earth by creating polyatomic allotropes of hydrogen with the aid of electricity and pressure, then subjecting the polyatomic allotropes of hydrogen to further pressure and electricity to induce nuclear fusion or nuclear transmutations.

The extreme heat of the sun is most likely a by-product of the nuclear fusion reactions in the sun rather than heat as an initiating mechanism of nuclear fusion reaction.

CONCLUSION

The existence of triatomic deuterium molecule or polyatomic allotropes of hydrogen in general is significant to fuel science because these polyatomic allotropes of hydrogen increase the probability of nuclear fusion and therefore, a sustainable production of nuclear energy through nuclear fusion will be available to mankind.

We have to invent the concept of "alpha bond" or "mono-electon bond" to account the theoretical existence of polyatomic allotropes of hydrogen and in order to account nuclear fusion reactions in the high-density sun. Nuclear fusion in the sun is not possible if only monoatomic atoms exist in the sun since monoatomic atoms are very far apart. There has to be polyatomic allotropes of hydrogen in the sun since polyatomic allotropes of hydrogen (D*3, D*4, D*5, etc.) increase the probability of nuclear fusion by virtue of the close distance of hydrogen atoms in a polyatomic structure.

Perhaps, we have to say good-bye to Hans Bethe's theory of energy mechanism of the sun and replace it by the author's new energy mechanism of the sun.

REFERENCE

1. Angus Andrew (1999). "A Mathematical Model of K Capture and Its Implications". Paper presented as poster in the *10th International Symposium on Capture Gamma Ray and Spectroscopy* in Sta. Fe, New Mexico, U.S.A. last August 30-September 3, 1999.

2. Krane, Kenneth (1983). "The Hydrogen Molecule Ion". In: *Modern Physics.* U.S.A.: John Wiley and Sons. pp. 360-364.

3. Krane, Kenneth (1983). "The Stellar Evolution". In: *Modern Physics.* U.S.A.: John Wiley and Sons. pp. 446-449.

4. Halliday, David and Resnick, Robert (1986). "Thermonuclear Fusion in the Sun and Other Stars". In: *Physics Part 2.* U.S.A.: John Wiley and Sons. pp.1317-1321.

5. Masterton, William L., Slowinski, Emil J., Stanitski C. (1985). *Chemical Principles.* 6th edition. U.S.A.: Saunders College Publishing. p.267